

Universality in the Anticoncentration of Noisy Quantum Circuits at Finite Depths

Arman Sauliere ,¹ Guglielmo Lami ,¹ Corentin Boyer ,¹ Jacopo De Nardis ,¹ and Andrea De Luca ¹

¹*Laboratoire de Physique Théorique et Modélisation, CNRS UMR 8089, CY Cergy Paris Université, 95302 Cergy-Pontoise Cedex, France*

We present universal properties of the anticoncentration of noisy quantum circuits at finite depth. By employing an effective model of *random matrix product operator*, we show that in the weak-noise regime different types of noise act in a similar fashion, leading to a universal distribution of bit-string probabilities, largely independent of the specific noise channel or circuit architecture. We identify three distinct depth-dependent regimes, each signaled by a different scaling of cross-entropy benchmarking (XEB) over rescaled depth. In the shallow-depth regime, noise effects are perturbatively small; in the intermediate regime, circuit-induced fluctuations and noise compete on equal footing; and in the deep-depth regime, the output distribution becomes effectively classical, up to corrections that are exponentially small in the noise strength. We provide quantitative predictions for the anticoncentration of generic circuits at finite depth, which we benchmark with numerical simulations displaying perfect agreement even for shallow circuits. Moreover, we show that, contrary to previous belief, the late-time XEB does give access to the global circuit fidelity, even for large noise strengths. Our findings are directly applicable to current quantum processors and demonstrate universal behavior beyond pure random-matrix-theory regimes which are only applicable at large depths.

I. INTRODUCTION

Quantum machines have transformative potential in many scientific fields, but current and near-term devices remain limited by external noise [1–11]. Although advances reduce noise levels, only fault-tolerant error correction can effectively suppress errors [4, 12–16]. Meanwhile, the development of methods to characterize noisy quantum circuits and to benchmark their output remains crucial [17–25]. A widely used benchmarking technique is *random circuit sampling* (RCS), in which one samples bit-strings \mathbf{x} from the output density matrix ρ of a random quantum circuit U [1, 26–28]. By comparing the observed output statistics with those from an ideal (noise-free) classical simulation of the same circuit, one quantifies the hardware global fidelity. This procedure, known as *cross-entropy benchmarking* (XEB), is experimentally accessible and has attracted significant interest [1, 3, 29–32]. Since XEB compares two replicas of the system—one noisy and one ideal—it can be readily analyzed using effective circuit averaging techniques developed for random unitary circuits [33]. However, it captures only partial information about the *anticoncentration* properties of the output distribution in the computational basis [32, 34–47]. The latter are instead fully encoded in the so-called *probability-of-probabilities distribution* (PoP) [1, 48, 49] $P(w)$, i.e. the average distribution of output probabilities $w = D\langle \mathbf{x} | \rho | \mathbf{x} \rangle$ (for convenience rescaled by the Hilbert space dimension D). The moments of the PoP are proportional to the celebrated *Inverse Participation Ratios* (IPR), often used to signal localization and non-ergodicity effects [50, 51].

In the absence of noise, the PoP for Haar-random quantum states follows the Porter–Thomas (PT) distribution [52], that for $D \rightarrow \infty$ takes the simple form $P_{\text{PT}}(w) = e^{-w}$. The same distribution is obtained for generic circuits of sufficiently large depth in the absence

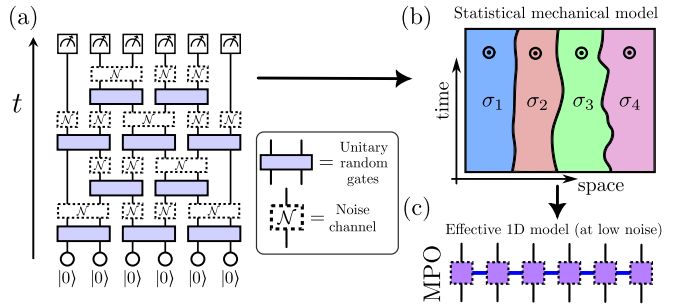


Figure 1. Sketch of the work. (a) We consider the task of random circuit sampling. The circuit is composed by random unitary gates in the usual brickwall geometry, and it is affected by noise represented by a quantum channel \mathcal{N} . We explore noise acting either on single or two-adjacent qubits, all yielding similar conclusions. (b) Theoretical arguments show that the gate average of the replicated circuit gives rise to an effective one-dimensional statistical model of permutations. In this model, noise acts as an external field that biases the system toward permutations close to the identity. (c) As a result, the original spatio-temporal circuit becomes equivalent to a one-dimensional random Matrix Product Operator (MPO) which incorporate noise.

of any conserved quantities. By contrast, generic classical stochastic processes produce uniform bit-string sampling, implying $P_C(w) = \delta(w-1)$, a distribution that also characterizes quantum devices overwhelmed by noise. In general, a noisy quantum circuit is expected to interpolate between these two extremes as a function of the noise strength. Additionally, these forms hold strictly in the infinite-depth limit [1, 48, 49]; capturing the quantum–classical crossover requires incorporating finite-depth corrections.

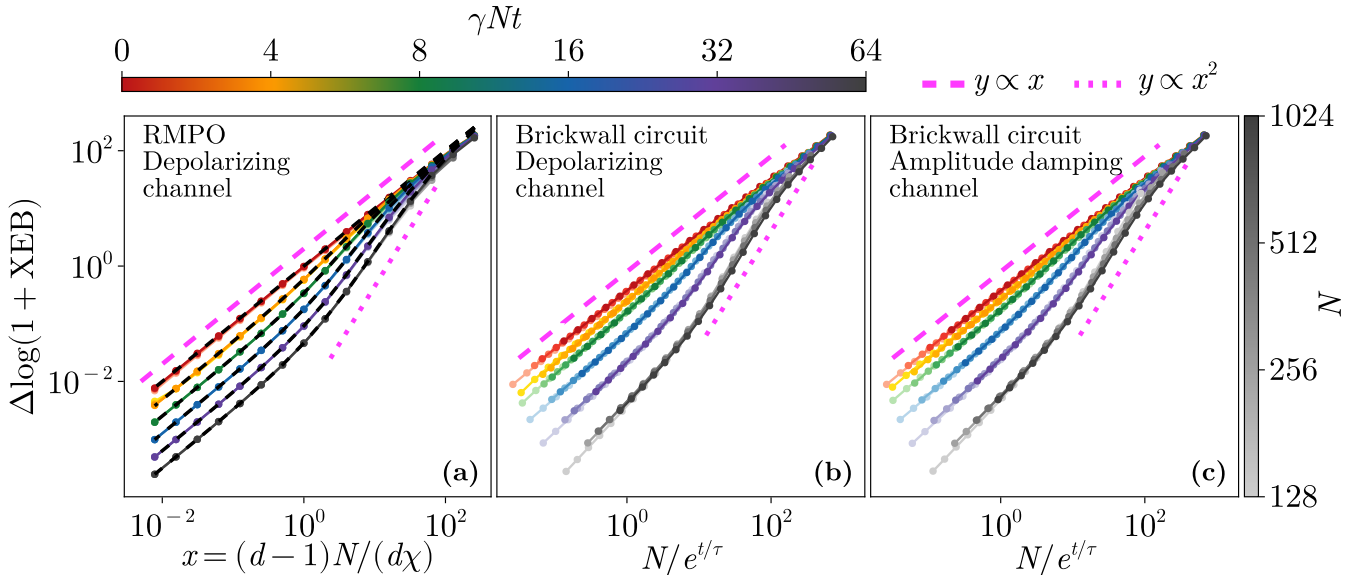


Figure 2. Plot of the XEB for noisy RMPO (a), and random brickwall circuits (b)-(c). Different noise models are considered: RMPO with depolarizing channel see Eq. (15), (a), random brickwall circuits with two-qubit depolarizing noise (b), or single-qubit amplitude damping noise (c). The noise strength is $\gamma \propto 1/(Nr)$ for RMPO (a), or $\gamma \propto 1/(Nt)$ for the circuit (b)-(c). The proportionality constant is indicated by the horizontal color bar at the top. Note that in panel (a), the label is γNr rather than γNt . We plot $\Delta \log(1 + \text{XEB}) = \log(1 + \text{XEB}) - \lim_{x \rightarrow 0^+} \log(1 + \text{XEB})$ as a function of the rescaled circuit depth $x \sim Ne^{-t/\tau}$. We identify three different scaling regimes fixed by the fitting parameter $\eta = -\log F$. For $x \gg \eta$, the scaling is with x and is independent of η , showing that the system is effectively noiseless. Then for $x^2 \sim \eta$, the scaling is with x^2 , characteristic of strong noise. For $x < 1$, it goes to its asymptotic value as a linear function of x . In panel (a) we also plot the prediction of Eq. (33) (dashed black line).

II. SUMMARY OF RESULTS

In this paper, we analyze the combined effects of finite depth and noise on both the XEB and the full PoP distribution in 1+1 dimensional quantum circuits with open boundary conditions. We focus on the weak-noise regime [29, 53], where η , the total number of errors in the circuit, is *intensive*. Although the number of error η can also increase with circuit depth, it remains subleading in N in many practical applications, and our assumption is therefore relevant. We show the existence of a *scaling regime* in the XEB and PoP distributions under *generic forms of noise*, in the weak-noise regime, characterized by two generic parameters: the parameter η , directly related to the global fidelity of the circuit $F = e^{-\eta}$, and the rescaled inverse circuit depth

$$x = \frac{N}{L(t)}, \quad L(t) = L_0 e^{t/\tau}, \quad (1)$$

where $L(t)$ is the characteristic length that governs the approach to random-matrix behavior (often dubbed Thouless length) [43, 44, 54–56]. The growth in time of this length, effectively a reparameterization of the circuit depth, is known to occur on the same timescale τ that governs the decay of the half-chain purity, which is $\sim e^{-t/\tau}$ [42, 44, 57]. Eq. (1) refers to a regime of shallow circuits, with $t = O(\log N)$. Within this scaling, we

identify *three dynamical regimes*, determined by the interplay between x and η , and fully characterize the PoP distribution $P_{x,\eta}(w)$ in each of them, thereby elucidating the quantum-to-classical crossover at finite depth. We obtain *universal results* arguing that in the weak noise limit and in the scaling limit 1, *generic circuits under different sources of noise can be reduced to effective Random matrix product operator (RMPO)*, which incorporate the noise, see also Fig. 1. Our construction of RMPO extends that of Random Matrix Product States (RMPS) [58–63] through a sequential quantum circuit, by formally doubling the Hilbert space and incorporating noisy channels. The mapping is established explicitly in the treatable example of the Random Phase Model (RPM) [44, 54] in the limit of large local Hilbert space dimension. We obtain explicit expressions for the XEB and for the moments of the outcome probabilities and introduce an effective numerical procedure to reconstruct the PoP. By extensive numerical simulations, we show that our scaling regime provides a useful quantitative description even for random circuits with brick wall geometry, paradigmatic models of quantum many-body chaotic systems [33, 64–75], with different forms of realistic experimental noise.

We then consider the situation where the number of errors scales with circuit depth $\eta = \lambda t$, in the regimes where our results remain valid. We use them to find a

universal form of XEB at a late time that well explains the observed transition in its decay rate as a function of the noise strength [3]. Nonetheless, we show that it can still be used to extract the global fidelity of the circuit for generic noise strength.

Our results therefore provide a unified framework for understanding how noise and finite depth jointly shape the benchmarking metrics of near-term quantum processors.

III. SETUP AND METHODS

We consider a system of N qudits of local dimension d , with total Hilbert space dimension $D = d^N$. The computational basis is labeled by bit strings $|\mathbf{x}\rangle = |x_1, \dots, x_N\rangle$, where $x_i \in \{0, \dots, d-1\}$. The task of *Random Circuit Sampling* (RCS) is to apply a random (but fixed) quantum circuit U to the initial state $|0\rangle = |0, \dots, 0\rangle$, which yields $\rho(U) = U|0\rangle\langle 0|U^\dagger$, and then to sample bit-strings \mathbf{x} from the *output distribution* $p(\mathbf{x}; \rho(U))$, where we define

$$p(\mathbf{x}; \rho) := \langle \mathbf{x} | \rho | \mathbf{x} \rangle. \quad (2)$$

To fix ideas, we consider a brickwall circuit with alternating layers of two-qudit gates, all independently drawn from the Haar measure $\text{Haar}(d^2)$ (see Fig. 1).

In realistic settings, these gates are subject to noise, modeled by a quantum channel of the form

$$\mathcal{N}(\rho) = \sum_{\alpha} K_{\alpha} \rho K_{\alpha}^\dagger, \quad \sum_{\alpha} K_{\alpha}^\dagger K_{\alpha} = \mathbb{1} \quad (3)$$

where K_{α} are Kraus operators.

We introduce a formal microscopic positive parameter, γ , which quantifies the *strength* of the noise channel \mathcal{N} . Consequently, both the channel and its Kraus operators depend explicitly on this parameter, i.e. $\mathcal{N} \rightarrow \mathcal{N}_{\gamma}$ and $K_{\alpha} \rightarrow K_{\alpha}(\gamma)$. For zero noise strength, $\gamma = 0$, the noise channel must reduce to the identity, namely $\lim_{\gamma \rightarrow 0^+} \mathcal{N}_{\gamma}(\rho) = \rho$, and therefore $\lim_{\gamma \rightarrow 0^+} K_{\alpha}(\gamma) = \delta_{\alpha,0} \mathbb{1}$. In next Section, we will utilize this reduction to the identity for a weak-noise expansion. As an explicit example, the depolarizing noise channel is given by $\mathcal{N}_{\gamma}^{\text{dep.}}(\rho) = (1 - \gamma)\rho + \gamma \frac{\mathbb{1}}{q}$, where $\gamma \in [0, 1]$ and q is the dimension of the Hilbert space on which the noisy channel acts. In general, we consider scenarios where the noise channels act on single qudits ($q = d$) or on multiple qudits (for example, two qudits where $q = d^2$). Under noise, the system evolves into a noisy version $\rho_{\mathcal{N}}(U)$ of the final state, and consequently the output distribution becomes $p(\mathbf{x}; \rho_{\mathcal{N}}(U))$.

A crucial quantity to measure the success in RCS is the *linear cross-entropy benchmark* (XEB)

$$\text{XEB}(U) = D \sum_{\mathbf{x}} p(\mathbf{x}; \rho_{\mathcal{N}}(U)) p(\mathbf{x}; \rho(U)) - 1, \quad (4)$$

which is the correlation between the ideal and the noisy distributions. For intermediate system sizes, the XEB

can be calculated by combining experimental data with a classical simulation [1] and, for deep circuits ($t \gg \log N$, i.e. $x \rightarrow 0$) has been used as a (experimentally-friendly) proxy for the fidelity $F(U) = \text{Tr}[\rho_{\mathcal{N}}(U)\rho(U)]$ between the ideal target state and its noisy counterpart, although some recent works pointed out that this may only be true when the noise is sufficiently weak [3, 29, 30, 76].

Other key quantities we analyze are the PoP and its moments, represented by the *Inverse Participation Ratios* (IPRs) [49], defined respectively as

$$\begin{aligned} P(w; U) &= D^{-1} \sum_{\mathbf{x}} \delta(w - D p(\mathbf{x}; \rho_{\mathcal{N}}(U))), \\ I_k(U) &= \sum_{\mathbf{x}} p(\mathbf{x}; \rho_{\mathcal{N}}(U))^k \quad \text{with } k \geq 1. \end{aligned} \quad (5)$$

These probe the anticoncentration of the final state in the computational basis. Up to a constant factor, the IPR equals the k -th moment of the PoP: $\mathbb{E}[w^k] = D^{k-1} I_k$.

While the quantities defined above depend explicitly on the specific circuit instance U , one can average them over an ensemble of random circuits, thereby defining $\text{XEB} = \mathbb{E}_U[\text{XEB}(U)]$, $F = \mathbb{E}_U[F(U)]$, $I_k = \mathbb{E}_U[I_k(U)]$, and $P(w) = \mathbb{E}_U[P(w; U)]$. To compute such circuit averages $\mathbb{E}_U[\dots]$, we employ Weingarten calculus [77, 78], which expresses the Haar average of k copies of a unitary gate as a sum over permutation operators $\sigma \in S_k$, where S_k is the symmetric group of order k . Specifically, using the vectorized representation of operators $O \rightarrow |O\rangle\langle O|$ and of their inner product $\text{tr}(O^\dagger Q) = \langle\langle O | Q \rangle\rangle$, the Weingarten formula reads [77, 78]

$$\mathbb{E}_{U \sim \text{Haar}(q)} [(U^* \otimes U)^{\otimes k}] = \sum_{\pi, \sigma \in S_k} \text{Wg}_{\pi, \sigma}(q) |\sigma\rangle\langle\langle \pi|. \quad (6)$$

Here, $\text{Wg}(q)$ denotes the $k! \times k!$ Weingarten matrix, which is the pseudo-inverse of the overlaps matrix $G_{\pi, \sigma}(q) := \langle\langle \pi | \sigma \rangle\rangle_q$ (subscript indicates the Hilbert space dimension). For a q -dimensional Hilbert space, vectorized permutations can be formally expanded in the computational basis as

$$|\sigma\rangle\langle\langle = \sum_{x_1, \dots, x_k=0}^{q-1} |x_1, x_{\sigma^{-1}(1)}\rangle\langle x_k, x_{\sigma^{-1}(k)}|. \quad (7)$$

We can graphically represent these states using the standard tensor network notation. For example, with $k = 4$ replicas, Eq.(7) for the permutation $\sigma = (1)(2 3 4)$ reads

$$|\sigma\rangle\langle\langle = \begin{array}{cccccccc} x_1 & x_1 & x_2 & x_4 & x_3 & x_2 & x_4 & x_3 \\ \cup & & \curvearrowright & & \curvearrowright & & \curvearrowright & \\ & & x_2 & x_4 & x_3 & x_2 & x_4 & x_3 \end{array} \quad (8)$$

where we explicitly label the indices represented by the lines. For large q , the overlap and Weingarten matrices can be expanded as

$$\begin{aligned} G(q) &= q^k (\mathbb{1} + q^{-1} A + O(q^{-2})) \\ \text{Wg}(q) &= q^{-k} (\mathbb{1} - q^{-1} A + O(q^{-2})), \end{aligned} \quad (9)$$

where the matrix A connects (with unit coefficient) only permutations differing by a single transposition.

Without noise and for global random unitaries $U \sim \text{Haar}(D)$, or equivalently circuits of sufficiently large depth, the PoP follows the well-known *Porter-Thomas* (PT) distribution

$$P_{\text{PT}}(w) = e^{-w}, \quad (10)$$

and correspondingly the IPRs are $I_k^{\text{PT}} = k!D^{1-k}$ (both equalities hold for $D \gg 1$). The absence of noise results in a perfect cross-entropy score $\text{XEB}_{\text{PT}} = DI_2 - 1 \simeq 2 - 1 = 1$.

To illustrate how noise disrupts these results, let us consider the simple scenario of a global depolarizing channel $\rho_{\text{noise}} = \mathcal{N}_{\gamma_{\text{glob}}}^{\text{dep.}}(U|\mathbf{0}\rangle\langle\mathbf{0}|U^\dagger)$, with $U \sim \text{Haar}(D)$ as before. In this case, the bitstring distribution is $p(\mathbf{x}; \rho_{\mathcal{N}}(U)) = (1 - \gamma_{\text{glob}})p(\mathbf{x}; \rho(U)) + \frac{\gamma_{\text{glob}}}{D}$, and therefore the IPR is $I_k(\gamma_{\text{glob}}) = D \sum_{j=0}^k \binom{k}{j} (1 - \gamma_{\text{glob}})^j \left(\frac{\gamma_{\text{glob}}}{D}\right)^{k-j} \mathbb{E}_U[p(\mathbf{0}; \rho(U))^j]$. Using the moments of the PT distribution, we have $\mathbb{E}_U[p(\mathbf{0}; \rho(U))^j] = j!D^{-j}$. Moreover, it is useful to expand the factorial as $j! = \sum_{i=0}^j i! \cdot \binom{j}{i}$, where $i!$ denotes the number of derangements of a set of size i , that is, the number of permutations with no fixed points [79]. Exchanging the sums over j and i yields $I_k(\gamma_{\text{glob}}) = D^{1-k} \text{Tr}[e^{Q \ln(1-\gamma_{\text{glob}})}]$, with

$$Q_{\sigma'\sigma} = \delta_{\sigma'\sigma} (k - n_F(\sigma)), \quad (11)$$

a diagonal $k! \times k!$ matrix that depends on the number of fixed points $n_F(\sigma)$ of the permutation, and plays a central role in our subsequent analysis. The weight $e^{Q \ln(1-\gamma_{\text{glob}})}$ favors permutations with more fixed points, and in the strong noise limit $\gamma_{\text{glob}} \rightarrow 1$, it suppresses all but the identity e (for which $Q_{ee} = 0$). The corresponding PoP is a *shifted Porter-Thomas* (SPT) distribution, given by

$$P_{\gamma_{\text{glob}}}^{\text{SPT}}(w) = (1 - \gamma_{\text{glob}})^{-1} e^{-\frac{w-\gamma_{\text{glob}}}{1-\gamma_{\text{glob}}}} \theta(w - \gamma_{\text{glob}}) \quad (12)$$

where $\theta(w)$ is the Heaviside function. The noise strength γ_{glob} is directly related to the goodness of the cross-entropy benchmarking, as $\text{XEB}_{\text{SPT}} = 1 - \gamma_{\text{glob}}$. In the strong noise limit $\gamma_{\text{glob}} \rightarrow 1$, the SPT distribution converges to $P_C(w) = \delta(w - 1)$, with corresponding IPRs $I_k^C = D^{1-k}$, reflecting the dominance of the identity permutation e over all others. This delta distribution $P_C(w)$ can thus be interpreted as the classical (i.e. non-quantum) form of the PoP.

IV. RANDOM MATRIX PRODUCT OPERATOR MODEL

We now consider local quantum circuits in a weak-noise regime where the total number of errors η remains $O(1)$. We shall first summarize the results for noiseless unitary evolution, i.e. $\eta \rightarrow 0$. It was recently argued that a universal form of the moments in the scaling limit at fixed x can be derived from an effective one-dimensional

model [44]. One way of understanding this is to formally represent the state $U|\mathbf{0}\rangle$ into an equivalent Matrix Product State (MPS), with the bond dimension $\chi \sim L(t)$, the Thouless length in Eq. (1), growing exponentially in the circuit depth t . Following the arguments of [44, 55], in the scaling limit (s.l.) $N, \chi \rightarrow \infty$ at fixed

$$x = \frac{d-1}{d} \frac{N}{\chi}, \quad (13)$$

we can expect that sampling from such time-evolved state is equivalent to sampling from a RMPS, i.e. one in which the local tensors are random and identically distributed (see below for a precise definition). Then, the k -replica average expresses the IPRs as the partition function of a 1D statistical mechanical model with local degrees of freedom in the permutation space [42–44]. Such a partition function can be expressed as a product of transfer matrices of size $k! \times k!$, ultimately related, in the scaling limit, to the matrix A introduced above, leading to

$$I_k \stackrel{\text{s.l.}}{=} D^{1-k} \langle 1 | e^{xA} | 1 \rangle = I_k^{\text{PT}} \exp\left(x \frac{k(k-1)}{2}\right). \quad (14)$$

with $|1\rangle = |1 \dots 1\rangle$ a boundary vector of length $k!$ (which is the eigenvector of the matrix A corresponding to its maximal eigenvalue). Finally, one can reconstruct the PoP distribution at any x by recognizing that the moments in Eq. (14) correspond to those of a product of two independent random variables, namely $w = w_{\text{PT}} g$, where w_{PT} is drawn from the Porter-Thomas distribution and g from a log-normal one (such that $\mathbb{E}[g^k] = \exp(xk(k-1)/2)$). These results coincide perfectly with those obtained for the RPM in the limit of large local Hilbert space dimension d [44]. More fundamentally, this reduction to an effectively 1D model is based on the idea that, after coarse-graining, in the space of replicas, the domain walls between adjacent permutations *extend vertically* along the entire depth of the circuit (see Fig. 1(b)): a fact that is ultimately a consequence of the membrane picture [33, 80–82].

We will show that this approach can be successfully extended to circuits in the presence of noise, yielding quantitative predictions for finite-depth circuits. To this end, and following the previous argument regarding the reduction to effective one-dimensional models, we model a generic noisy circuit as a noisy staircase quantum circuit.

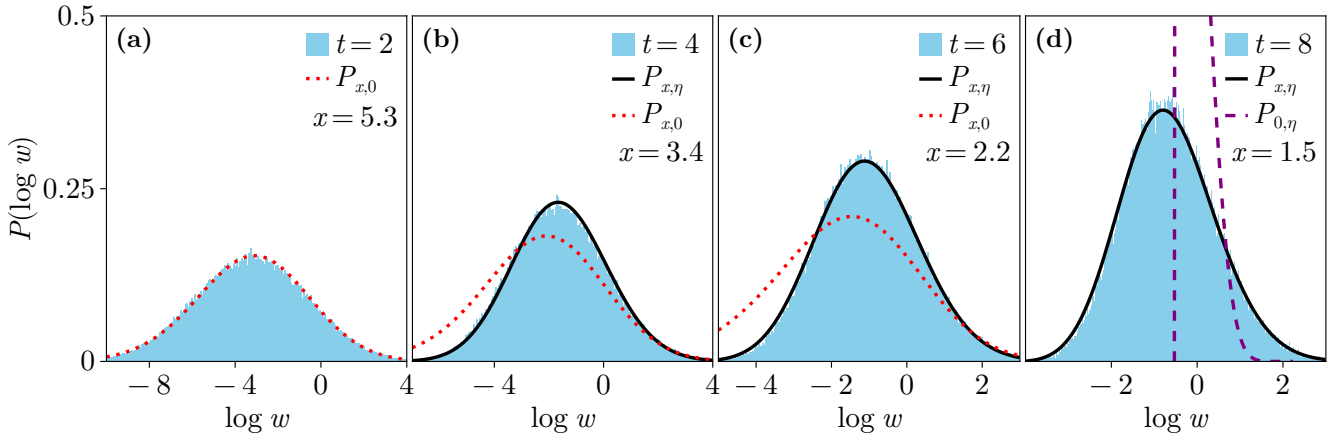
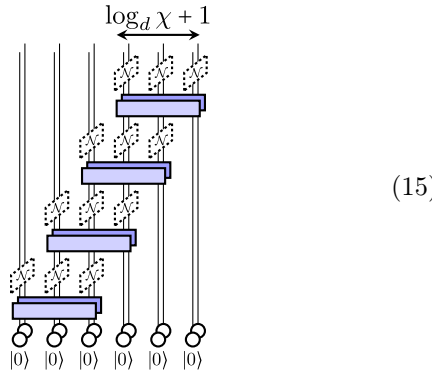


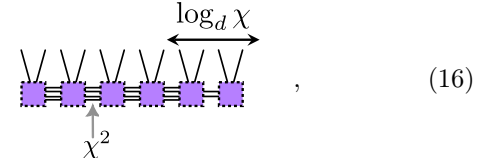
Figure 3. Plot of the PoP for a Haar-random brickwall circuit subject to two-qubit depolarizing noise with $\gamma Nt = 2$ and system size $N = 32$. Different depths t are explored (see values reported in the plots). At the shortest depth, the distribution is well approximated by the noiseless distribution (dotted red curve) $P_{x,0} \simeq P_{x,\eta}$, whereas the latter fails to accurately describe the data at larger depths. In contrast, the theoretically predicted distribution $P_{x,\eta}$ (black line) accurately reproduces the data. The Shifted Porter-Thomas (SPT), Eq. (12), corresponding to the distribution at infinite times, $x = 0$, is also plotted for reference in the last plot. The values of x and η are obtained by the fitting procedure involving the XEB data explained in the main text (sec. VI).

Specifically, our construction is as follows:



The unitary gates U_i in the staircase circuit act on $r+1$ qudits of local dimension d , where $r = \log_d \chi$ (for illustrative purpose, $r = 2$ in Eq. (15)). The full set of gates is denoted by $U := \{U_i\}_{i=1}^{N-r}$. In the absence of noise, Eq. (15) reduces to the standard sequential generation of an MPS of bond dimension χ , starting from qudits initialized in the state $|0\rangle$ [83]. In Eq. (15), unitary gates are interleaved with layers of single-qudit noise channels N_γ . For the moment, we do not need to specify the precise form of the noise channel beyond Eq. (3). Since N_γ acts on the density matrix, both the state and its conjugate are shown (with conjugate operators represented by darker shapes). Although we focus here on the model illustrated in Eq. (15), our results are *universal* and extend beyond this specific architecture. For instance, in Appendix C, we analyze the *Random Phase Model* (RPM) and demonstrate that it exhibits the same universal properties. Furthermore, in Appendix B, we show that extending the staircase circuit to include noise acting jointly on $r+1$ qudits in each layer, also leads to the

same universal description. Both this multi-qudit noise construction and the single-qudit noise architecture in Eq. (15) generate a mixed density matrix $\rho_N(U)$, which can be represented as a *Random Matrix Product Operator* (RMPO), see also Fig. 1. This becomes evident by suitably reshaping Eqs. (15) and by fusing each gate U_i and its conjugate U_i^* with the corresponding noise channels. This yields



which is in fact an MPO of bond dimension χ^2 , shown in its vectorized form (the bond dimension decreases by a factor d^2 after each of the last r sites near the right boundary).

To compute the overlap, Eq. (2), $w_{\mathbf{x}} = D\langle \mathbf{x} | \rho_N(U) | \mathbf{x} \rangle = D\langle \mathbf{x}, \mathbf{x} | \rho_N(U) \rangle$, the open physical legs in Eq. (15) should be contracted with a bit-string \mathbf{x} . Afterwards, to evaluate $I_k = D^{-k} \sum_{\mathbf{x}} \mathbb{E}_U[w_{\mathbf{x}}^k]$ one should replicate this network k times, and apply Eq. (6) to each of the unitary gates U_i in Eq. (15), each of which acts on a Hilbert space of dimension $d\chi$. Doing this, one can express the IPR I_k in terms of powers of an appropriate transfer matrix. Specifically, we arrive at (see details in the Appendix A)

$$I_k = (L|T^{N-r-1}|R), \quad (17)$$

where the transfer matrix

$$T := \Lambda(d, \gamma) \tilde{G}(\chi, \gamma) Wg(d\chi), \quad (18)$$

acts in the space of permutations, thus having size $k! \times k!$. The noise enters this transfer matrix in two ways. First, the matrix \tilde{G} is a noisy version of the usual overlap matrix $G_{\sigma'\sigma}(\chi) = \langle\langle \sigma'|\sigma\rangle\rangle_\chi$, defined as

$$\tilde{G}_{\sigma'\sigma}(\chi, \gamma) := \langle\!\langle \sigma' | \mathcal{N}_\gamma^{\otimes k} | \sigma \rangle\!\rangle_d^r. \quad (19)$$

It takes into account the effect of the noisy channels (of strength γ) placed between two consecutive unitary gates U_i, U_{i+1} in Eq. (15). Secondly, the diagonal matrix $\Lambda_{\sigma'\sigma}(d, \gamma) = \delta_{\sigma'\sigma} \sum_{x=0}^{d-1} (\langle x, x \rangle)^{\otimes k} \mathcal{N}_\gamma^{\otimes k} |\sigma\rangle \langle \sigma|_d$ encodes the action of the noise channel and projection on the basis state x for the leftmost qubits of each layer of the staircase circuit in Eq. (15). Finally, the boundary vectors in Eq. (17) read $|L\rangle = (1| \text{Wg}(d\chi)$ and $|R\rangle = \Lambda(d, \gamma)^{r+1} |1\rangle$. For small replica numbers k , Eq. (17) enables the exact evaluation of I_k for arbitrary noise channels, via direct multiplication of matrices of size $k! \times k!$.

We now proceed to analyze the weak-noise regime. We consider the standard expansion of the Kraus operators at first order in γ [84]

$$\begin{cases} K_0(\gamma) = \mathbb{1} - \gamma \tilde{K}_0 + O(\gamma^2). \\ K_\alpha(\gamma) = \sqrt{\gamma} \tilde{K}_\alpha + O(\gamma^{3/2}) \end{cases} \quad \text{for } \alpha \geq 1, \quad (20)$$

so that the action of the noisy channel becomes $\mathcal{N}_\gamma(\rho) = \sum_\alpha K_\alpha(\gamma)\rho K_\alpha^\dagger(\gamma) = \rho + \gamma\tilde{\mathcal{N}}(\rho) + O(\gamma^2)$, with

$$\tilde{\mathcal{N}}(\rho) = \sum_{\alpha \geq 1} \tilde{K}_\alpha \rho \tilde{K}_\alpha^\dagger - \tilde{K}_0 \rho - \rho \tilde{K}_0^\dagger. \quad (21)$$

The trace-preserving condition of the noise channel gives $\tilde{K}_0 + \tilde{K}_0^\dagger = \sum_{\alpha \geq 1} \tilde{K}_\alpha^\dagger \tilde{K}_\alpha$. The Kraus operators are not uniquely defined, and we can fix this freedom by choosing the \tilde{K}_α to be traceless.

We focus on the regime in which the noise strength γ decreases as the system size grows, according to a specific scaling limit. The scaling limit (s.l.) is defined as follows: first, in accordance with the noiseless case discussed above and Eq. (13), we keep $x = N/\chi \cdot (d-1)/d$ fixed as $N, \chi \rightarrow \infty$; second, we scale the noise strength as $\gamma \propto \eta/(Nr)$ where Nr is the total number of noise channels applied in Eq. (15) [85]. Notice that $\Lambda_{\sigma'\sigma}(d, \gamma) = \delta_{\sigma'\sigma} d (1 + O(\gamma))$, and that only $O(N)$ of these matrices are present in Eq. (17). Therefore, since $\gamma = O((Nr)^{-1})$, in the scaling limit Λ can be effectively replaced by the identity matrix (times d): $\Lambda_{\sigma'\sigma}(d, \gamma) \xrightarrow{\text{s.l.}} d \delta_{\sigma'\sigma}$.

While $\tilde{G}_{\sigma'\sigma}(\chi, \gamma)$ gives non-trivial noise-induced corrections, those affecting the off-diagonal elements are negligible in the scaling limit. In fact, these terms are already $O(\chi^{-1})$ at zero noise, because $\tilde{G}_{\sigma'\sigma}(\chi, 0) = \chi^k (\delta_{\sigma'\sigma} + \chi^{-1} A_{\sigma'\sigma} + O(\chi^{-2}))$ (see Eq. (9)). For example, a correction of order γ to the matrix A would be associated with a weight $O(\chi^{-1}\gamma)$, and thus would not contribute to the scaling limit. Hence, the only relevant corrections are those arising from the diagonal elements

of \tilde{G} . We have

$$\begin{aligned} \langle\langle \sigma | \mathcal{N}_\gamma^{\otimes k} | \sigma \rangle\rangle_d &= \\ &= d^k + \gamma \sum_{a=1}^k \langle\langle \sigma | \mathbb{1}^{\otimes(a-1)} \otimes \tilde{\mathcal{N}}_a \otimes \mathbb{1}^{\otimes(k-a)} | \sigma \rangle\rangle_d + O(\gamma^2), \end{aligned} \quad (22)$$

where the zeroth-order term arises from $\langle\langle\sigma|\sigma\rangle\rangle_d = d^k$, $\mathbb{1}$ is the identity super-operator, and the index $a \in \{1, \dots, k\}$ labels the replicas. Consider the matrix element $\langle\langle\sigma|\mathbb{1}^{\otimes(a-1)} \otimes \tilde{\mathcal{N}}_a \otimes \mathbb{1}^{\otimes(k-a)}|\sigma\rangle\rangle_d$ in the term of order $O(\gamma)$ on the right-hand side of Eq. (22). To visualize this quantity, we set for the moment $k = 4$, consider the specific permutation $\sigma = (1)(2\ 3\ 4)$, and use a graphical notation. If the noise channel $\tilde{\mathcal{N}}$ is placed on the first replica, i.e. the $a = 1$ term in the sum, then we have

$$\langle\langle\sigma|\tilde{\mathcal{N}}\otimes 1^{\otimes 3}|\sigma\rangle\rangle_d = \tilde{\mathcal{N}} \text{ [shaded box]} \text{ [bra-ket]} \text{ [ket]} . \quad (23)$$

where the permutation σ has been folded as in Eq. (8). We observe that since $a = 1$ corresponds to a fixed point of the permutation σ , i.e. $\sigma(a) = a$, then Eq. (23) contains the factor

$$\tilde{\mathcal{N}} \cdot \text{[Diagram 24]} = \langle\langle e | \tilde{\mathcal{N}} | e \rangle\rangle_d = \text{Tr}[\tilde{\mathcal{N}}(\mathbb{1})] = 0. \quad (24)$$

Therefore, all fixed points of σ yield a vanishing contribution in the summation in Eq. (22). Conversely, when the noise channel \mathcal{N} acts on a replica that is not a fixed point of σ , i.e. $\sigma(a) \neq a$, non-vanishing contributions arise. For example, by setting $a = 2$ we obtain the matrix element

$$\langle\langle \sigma | 1 \otimes \tilde{\mathcal{N}} \otimes 1^{\otimes 2} | \sigma \rangle\rangle_d = \langle\langle \sigma | \tilde{\mathcal{N}} | \sigma \rangle\rangle \quad . \quad (25)$$

This term is proportional to

$$\begin{aligned}
 \left(\begin{array}{c} \text{---} \\ \text{---} \\ \text{---} \\ \text{---} \end{array} \right) \tilde{N} \left(\begin{array}{c} \text{---} \\ \text{---} \\ \text{---} \\ \text{---} \end{array} \right) &= \sum_{\alpha \geq 1} \text{Tr}[\tilde{K}_\alpha] \text{Tr}[\tilde{K}_\alpha^\dagger] - d \text{Tr}[\tilde{K}_0] - d \text{Tr}[\tilde{K}_0^\dagger] = \\
 &= -d \sum_{\alpha \geq 1} \text{Tr}[\tilde{K}_\alpha^\dagger \tilde{K}_\alpha], \tag{26}
 \end{aligned}$$

where we used that \tilde{K}_α are traceless and the trace-preserving condition for \tilde{K}_0 . The proportionality constant can be determined by noting that the noise channel

acts as the identity on the remaining $k - 2$ lines leading to a factor d^{k-2} . For instance, Eq. (25), with $k = 4$, includes the term in Eq. (26) along with two additional loops, each corresponding to a free index summed over d values, thus giving a total factor $d^2 = d^{k-2}$. Combining these observations, we obtain

$$\begin{aligned} \sum_{a=1}^k \langle\langle \sigma | \mathbb{1}^{\otimes(a-1)} \otimes \tilde{\mathcal{N}}_a \otimes \mathbb{1}^{\otimes(k-a)} | \sigma \rangle\rangle_d &= \\ = -d^{k-1} \left(\sum_{\alpha \geq 1} \text{Tr}[\tilde{K}_\alpha^\dagger \tilde{K}_\alpha] \right) \sum_{a=1}^k (1 - \delta_{a,\sigma(a)}) & \quad (27) \\ = -d^{k-1} \left(\sum_{\alpha \geq 1} \text{Tr}[\tilde{K}_\alpha^\dagger \tilde{K}_\alpha] \right) (k - n_F(\sigma)). \end{aligned}$$

Including also the expansion of the off-diagonal terms of \tilde{G} , which coincides with the zero-noise case, we obtain

$$\tilde{G}(\chi, \gamma) = \chi^k \left(1 + \frac{d}{d-1} \frac{x}{N} A - \frac{\eta}{N} Q + O(N^{-2}) \right), \quad (28)$$

with the matrices A and Q defined in Eqs. (9) and (11) respectively, and where we used the definition of x from Eq. (13) and we fixed the noise strength in terms of the parameter η as

$$\gamma = \frac{\eta}{Nr} d \left(\sum_{\alpha \geq 1} \text{Tr}[\tilde{K}_\alpha^\dagger \tilde{K}_\alpha] \right)^{-1}. \quad (29)$$

Notice that γ is necessarily positive, since $\tilde{K}_\alpha^\dagger \tilde{K}_\alpha$ is a positive matrix. For example, considering the depolarizing channel $\mathcal{N}_\gamma^{\text{dep.}}(\rho) = (1-\gamma)\rho + \gamma \frac{1}{d} = \rho + \gamma \tilde{\mathcal{N}}^{\text{dep.}}(\rho)$, with, in vectorized form, $\tilde{\mathcal{N}}^{\text{dep.}} = -\mathbb{1} + \frac{1}{d}|e\rangle\langle e|$, with $|e\rangle$ the singlet (or identity permutation), from which one can easily find $\text{Tr}[\tilde{K}_\alpha^\dagger \tilde{K}_\alpha] = \frac{d^2-1}{d}$. Finally, using Eq. (28) and Eq. (9), we find

$$\tilde{G}(\chi, \gamma) \text{Wg}(d\chi) = d^{-k} \left(1 + \frac{x}{N} A - \frac{\eta}{N} Q + O(N^{-2}) \right). \quad (30)$$

By using this equality and neglecting all terms $O(N^{-2})$, which are irrelevant in the scaling limit, we finally arrive at the expression for the transfer matrix

$$T \stackrel{\text{s.l.}}{=} d^{1-k} \exp \left(\frac{x}{N} A - \frac{\eta}{N} Q \right). \quad (31)$$

We should stress that our weak-noise expansion leading to Eq. (31) is completely *independent of the specific details of the noise, including whether the channel \mathcal{N} is unital or not*. By using this equation and taking the scaling limit, Eq. (17) reduces to

$$I_k \stackrel{\text{s.l.}}{=} I_k(x, \eta) := D^{1-k} (1|e^{xA-\eta Q}|1). \quad (32)$$

The form (32) for IPRs is one of the main results of this paper. Consistently, it reduces to the noiseless case Eq. (14) when $\eta = 0$. As in that case, it effectively describes the partition function of a 1D gas of domain walls

in the space of permutations, with x representing the fugacity. The parameter η , associated with noise, effectively plays the role of a magnetic field favoring permutations with larger number of fixed points (thus closer to the identity e).

The universality of Eq. (32) is based on two facts: first, as it happens in the noiseless case, in the scaling regime we consider, the domain walls are effectively diluted and only the elementary ones (transpositions) associated with the matrix A are relevant; secondly, while noise generally favours the identity permutation, we see that the generic measure of distance from the identity emerging in the weak-noise expansion is just associated to the number of fixed points. The latter is a bulk property that we expect not to affect the cost associated with domain-wall interfaces. Thus, only two parameters x, η encode for all the microscopic interactions and specific form of the noise, where the variable x is still expressed in terms of the Thouless length (Eq. (13)), in turn linked to the half-chain purity of the noiseless model: this hypothesis is verified in the models we solve analytically and in the numerical data we show below.

Note that in our RMPO model, Eq. (15), approximately r noise channels are applied per site. As a result, the total number of noise gates scales as $N_g \propto Nr$, and $\gamma \propto \eta/(Nr)$. In a realistic quantum circuit extended in time, the number of errors is naturally proportional to the circuit depth. In that case, the time variable t plays the role of r , leading to $N_g \sim Nt$. The relevance of our results for this case will be addressed in Section VII.

The PoP $P_{x,\eta}(w)$ is uniquely determined by the moments Eq. (32). In the noiseless case ($\eta = 0$), Eq. (32) reduces to Eq. (14) and $P_{x,0}(w)$ is a log-normal convolved with PT. Moreover, for infinite circuit depth ($x = 0$), one recovers the moments of the SPT distribution Eq. (12) (see previous section). Thus, Eq. (32) interpolates between these two regimes, capturing the combined effects of noise and finite depth through the scaling parameters η and x . For small k , Eq. (32) provides an efficient way to compute the scaling form of the IPRs for arbitrary x, η . In particular, in the same framework and scaling limit, we can derive a closed form for the XEB, as it is closely related to I_2 . Technically, the discrepancy between XEB and I_2 lies in the fact that in Eq. (4) only one of the two replicas contains noise, thus leading to

$$\begin{aligned} \text{XEB} &\stackrel{\text{s.l.}}{=} (1|e^{xA-\frac{\eta}{2}Q}|1) - 1 = \\ &= 2e^{-\eta/2} \left[\cosh(\theta(x, \eta)) + \frac{x \sinh(\theta(x, \eta))}{\theta(x, \eta)} \right] - 1, \end{aligned} \quad (33)$$

where $\theta(x, \eta) = \sqrt{x^2 + (\eta/2)^2}$. For $x = 0$, the XEB gives back the circuit fidelity F as expected from the white noise approximation that becomes valid in the limit of weak noise [53]. In fact, we find (see Appendix A for the explicit calculation of the average fidelity):

$$\lim_{x \rightarrow 0^+} \text{XEB} = e^{-\eta} = F. \quad (34)$$

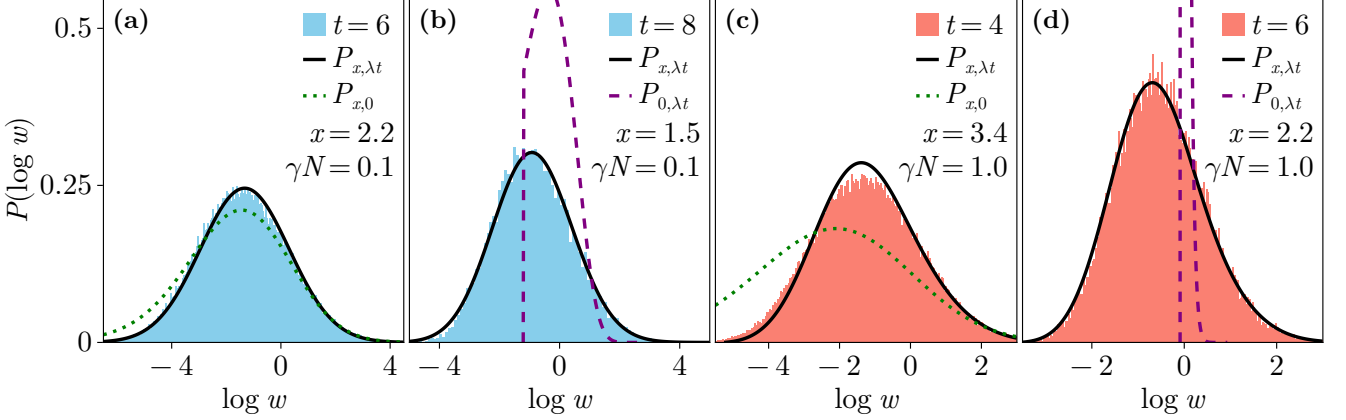


Figure 4. Plot of the PoP for a Haar-random brickwall circuit subject to two-qubit depolarizing noise with two different values of γN and $N = 32$. We present both $\gamma N = 0.1$ in (a),(b), and $\gamma N = 1.0$ (c),(d). For each value of γN , we consider two different depths t , and consequently x (see values reported in the plots), corresponding to two different regimes of the XEB (see Eq. (39)), (a) $\lambda < 1/\tau$ and (b) $\lambda > 1/\tau$. The values of x and λ are obtained by the fitting procedure involving the XEB data explained in the main text (sec. VII).

This relation shows that generically the parameter η is fixed by the global fidelity of the circuit. The parameter x , is fixed by the system size and the spreading of purity in the noiseless circuit, see Eq. (1) and also Fig. 8. In the case of a one-dimensional Haar random brickwall circuit with d -dimensional qudits, the scaling of the purity is [86]

$$\tau_{\text{bw}}^{-1}(d) = \log\left(\frac{d^2 + 1}{2d}\right), \quad (35)$$

which for qubits gives $\tau_{\text{bw}}^{-1}(2) \simeq 0.223$.

In contrast to the $\eta = 0$ case, an analytic calculation for arbitrary k of the moments (Eq. (32)) from which to reconstruct the explicit form of the distribution is technically complex. Nonetheless, the behavior of the IPRs in different regimes of x can be extracted perturbatively as we show below. Additionally, we provide an effective numerical procedure to extract the PoP.

V. THE THREE DYNAMICAL REGIMES

For fixed η , Eqs. (32) and (33) reveal three distinct dynamical regimes as the circuit depth, and hence x , is varied, and which are manifested from the scaling of the XEB, see Fig. 2. These can be naturally grouped into a short-depth case and an intermediate-to-long-depth one. Notice that, for practical reasons, we define the deviation from the asymptotic value of the XEB in log-scale as $\Delta \log(1 + \text{XEB}) := \log(1 + \text{XEB}) - \lim_{x \rightarrow 0^+} \log(1 + \text{XEB})$.

Short-depth $x \gg \eta$. A simple inspection of Eq. (33) shows that $\Delta \log(1 + \text{XEB}) \propto x$ in this regime. Instead, Eq. (32) can be analyzed using perturbation theory in the small parameter η/x , expanding around the noiseless limit $\eta = 0$ (Eq. (14)). At first order, we find

$I_k \simeq I_k^{\text{PT}} \exp\left(x \frac{k(k-1)}{2} - \eta(k-1) + O(\eta^2/x)\right)$. The fact that the right-hand side of this expression does not yield $\lim_{k \rightarrow 0} I_k = D$, as it trivially should according to the definition in Eq. (5), indicates that the first-order expansion at small η/x cannot be analytically continued to $k < 1$. Nevertheless, it allows us to extract the PoP tails at $w \gg 1$ as a convolution of the PT with a (unnormalized) lognormal.

Large/intermediate-depth. To simplify the analysis, we assume that η is large enough that we can focus in practice only on the ground state of Q , which consists of the identity permutation e , perturbed by the matrix A . Without perturbation, and neglecting terms of order $O(e^{-2\eta})$, one simply obtains the classical value of the IPR, I_k^C . The perturbation introduces two relevant types of corrections. First, from second-order perturbation theory, one can obtain the correction: $x^2/(2\eta) \sum_{\sigma} A_{e,\sigma}^2 = x^2 k(k-1)/(4\eta)$. This expression can be interpreted as describing a region in the bulk where the state is locally excited to σ instead of remaining in the ground state e . This excited region is bounded by two domain walls, corresponding to identical transpositions that separate it from the surrounding ground state regions. Pictorially, we can represent this correction as follows:

$$\overbrace{\quad \quad \quad}^e \overbrace{\quad \quad \quad}^{\sigma} \overbrace{\quad \quad \quad}^e \quad (36)$$

Second, the boundary state $|1\rangle$ in Eq. (32) contains contributions from all permutations. As a result, transpositions σ can remain localized near the left or right boundaries before the perturbation given by the A matrix causes them to ‘jump’ to the ground state e , creating a domain wall at cost $O(x)$. This correction can be pic-

torially represented as



$$e \quad \sigma \quad (37)$$

and similarly on the left boundary. Putting these two contributions together, we arrive at $I_k = I_k^C \exp\left(\frac{x^2 k(k-1)}{\eta^2}\right) \left(1 + \frac{x k(k-1)}{\eta^2} + O(x^2/\eta^2)\right)$. The first term of this expression again indicates a log-normal PoP (the convolution with the delta distribution $P_C(w)$ is irrelevant). This expression also determines two distinct regimes by increasing the depth of the circuit (decreasing x). When $1 \ll x = \sqrt{\eta} \ll \eta$, the exponential factor dominates giving rise to $\log \mathbb{E}[w^k] \propto x^2/\eta^2$ behavior. In contrast, at larger depths for which $x \ll 1$, $\log \mathbb{E}[w^k] \propto x/\eta$. This behavior is explicitly confirmed by the analytical expression of the XEB (33).

The existence of these dynamic regimes is a direct consequence of the universal form (32). Fig. 2 presents numerical results for both noisy RMPO and random brickwall circuits confirming this analysis. For the brickwall circuit, we consider two types of noise: a two-qubit depolarizing channel and a single-qubit amplitude damping channel $\mathcal{N}_\gamma^{\text{amp.}}(\rho) = K_0 \rho K_0^\dagger + K_1 \rho K_1^\dagger$ with $K_0 = \begin{pmatrix} 1 & 0 \\ 0 & \sqrt{1-\gamma} \end{pmatrix}$ and $K_1 = \begin{pmatrix} 0 & \sqrt{\gamma} \\ 0 & 0 \end{pmatrix}$. Notably, the latter is non-unital, confirming that the emergence of these regimes does not depend on the unitality of the noise. We compute XEB by contracting the tensor network obtained by replicating the system and averaging all the unitary gates. The resulting replica tensor network lives in a $k!$ -dimensional space, spanned by the permutations; for $k = 2$, which is the case for XEB, a basis is given by the identity e and the transposition $s = (12)$. While for RMPS (and RMPO) the exact form of the rescaled depth $x = (N/\chi)(d-1)/d$ is derived analytically above, for the circuit we take the definition (1) and fit the parameter L_0 (the value of τ is provided in Eq. (35) but it could also be fitted). We plot $\Delta \log(1 + \text{XEB})$ as a function of x , or $N/e^{t/\tau}$ (circuit). For the circuit, we observe that plotting as a function of this variable yields good collapse of the curves corresponding to different system sizes N . Consistently, in all three cases, we clearly observe the predicted three regimes $O(x)$, $O(x^2)$ and $O(x)$.

VI. UNIVERSAL FORM OF THE POP DISTRIBUTION

The full PoP $P_{x,\eta}(w)$, defined by the moments in Eq. (32), is *universal* and determined only by the parameters x and η . In generic cases, these should be regarded as model-dependent fitting parameters (while for RMPO their explicit form in terms of χ , N , d and γ is known, see Eqs. (13) and (29)). To show the universality of this form, in Fig. 3 we compare the distribution arising

from our formula Eq. (32) (black lines) with the empirical distribution obtained by computing the overlaps w of random bit-strings with the final state in a Haar random brickwall circuit with two-qubit depolarizing noise (blue histogram) on each gate. The numerical data are obtained with tensor network simulations [87–90] with fixed N and $\gamma N t$ on each two-site gate, while we explore different values of depth t . Extracting the exact value of x and η is nontrivial due to the absence of analytical expressions for them in the brickwall circuit.

We here devise an experimentally friendly approach to access the parameters x and η in a generic circuit at a given finite depth. We compute the XEB (as it can be also done in an experimental setting) and extract η by extrapolating its value at large depth (ideally $x = 0$). Afterwards, we obtain x by setting Eq. (33) equal to the numerically (experimentally) obtained XEB data. These parameters are then used for the full distribution $P_{x,\eta}(w)$ with moments (32). The fact that the x and the η extracted just from the XEB provide good agreement is a non-trivial manifestation that all the moments of the anticoncentration follow the same universal form which depends only on these two parameters. We also confirm this with an extra check of reconstructing the I_3 moment from the XEB (see Fig. 7 in Appendix D).

A full analytical expression for the distribution $P_{x,\eta}$ from the moments (32) remains unfortunately inaccessible in a closed mathematical form for generic x and η . Using that for sufficiently large $\eta \gg x$, the distribution approaches a log-normal, namely a Gaussian in the variable $\log w$, allows for a systematic expansion. Specifically, we employ the Gram-Charlier A series [91, 92], which approximate a probability distribution in terms of its cumulants. The latter are computed numerically from Eq. (32) for $k \in \{1, 2, 3, 4, 5, 6\}$. In Fig. 3, the empirical distribution and our analytical prediction shows excellent agreement, with small deviations only due the finite size N of the simulation. Dotted red line represents the noiseless distribution $P_{x,0}(w)$ (log-normal convolved with PT), which closely match the empirical distribution for short time t (i.e. $x \gg 1$). At late time instead the distribution tends toward a Shifted Porter Thomas, i.e. $P_{0,\eta}(w)$ (purple dashed line).

VII. CIRCUITS WITH FIXED NOISE RATE IN TIME AND XEB TRANSITION

We shall now consider a more realistic scenario in which the noise strength γ does not scale inversely to the circuit depth t , but still decreases with the system size N . This corresponds to setting $\gamma = O(N^{-1})$, so that the total number of errors scales linearly with time, i.e. $\eta = O(t)$. Specifically, we define

$$\eta = \lambda t, \quad (38)$$

with fixed λ , related to the global fidelity, as before, via $F = e^{-\lambda t}$. All our results remain applicable in the regime

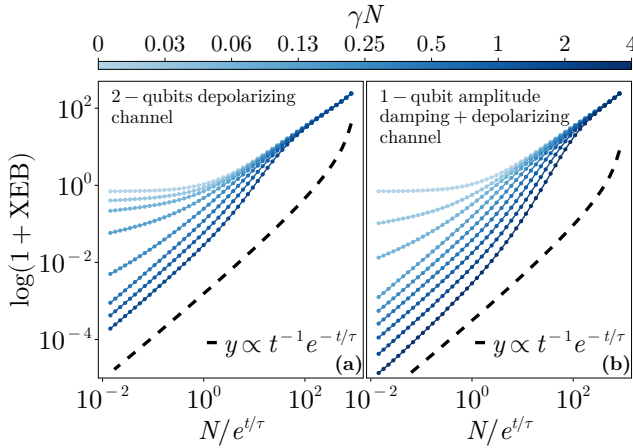


Figure 5. Plot of the XEB for the brickwall circuit with (a) two-qubits depolarizing (b) single-qubit amplitude damping and depolarizing channels, with different γN , and $N = 1024$. We observe the transition at large times in the scaling of $\log(1 + \text{XEB})$, from $-\lambda t$ to $-t/\tau$ as the noise strength γN is increased. The crossing happens at $\lambda = 1/\tau$ as predicted by Eq. (39) ($\tau = \tau_{\text{bw}}(2)$ in this model). In the regime $\lambda > 1/\tau$, while the slope of the decay is fixed by the noise-independent τ , a shift proportional to $1/\lambda$ as predicted by Eq. (39) is clearly visible, the latter allowing to determine the global fidelity.

$\lambda t \ll N$, namely whenever the total number of errors remain subleading. Expanding Eq. (33) for the XEB in the small- x limit, retaining only the first-order term in x , substituting $\eta \rightarrow \lambda t$, and using $x = e^{-t/\tau} \cdot N/L_0$, we obtain

$$\text{XEB} = e^{-\lambda t} + 2 \frac{e^{-t/\tau} N}{\lambda t} + O(x^2). \quad (39)$$

This expression can be easily interpreted viewing XEB as the partition function of a 1D system of size N in permutation space, expressed by (see first line of Eq. (33)): $\text{XEB} = (1 | (\exp(\frac{x}{N} A) \exp(-\frac{1}{2} \frac{\lambda t}{N} Q))^N | 1) - 1$. As the XEB is a quantity expressed only in terms of two replicas, the permutation space is limited to identity e and swap s . The term $\exp(-\frac{1}{2} \frac{\lambda t}{N} Q)$ weights each site with a factor 1 for identity and $\exp(-\frac{\lambda t}{N})$ for the swap. Each domain wall between the two permutations carry a factor $x/N = L^{-1}(t) = L_0^{-1} e^{-t/\tau}$, therefore at large times (i.e., for small x), domain walls between different permutations are suppressed. In this limit, the leading contributions come from configurations where the permutation is uniform across the system. There are two such trivial contributions. The configuration in which the permutation is e is exactly canceled by the -1 in the definition of XEB. The configuration where the permutation is s , or pictorially

$$\overbrace{\hspace{1cm}}^s, \quad (40)$$

yields $(\exp(-\frac{\lambda t}{N}))^N = e^{-\lambda t}$, i.e. the first term in Eq. (39). The second term in Eq. (39) (of order x) corresponds to

the configurations with a single domain wall

$$\overbrace{\hspace{1cm}}^e \overbrace{\hspace{1cm}}^s \quad \overbrace{\hspace{1cm}}^s \overbrace{\hspace{1cm}}^e \quad (41)$$

In fact, each of these contributes to a term $L^{-1} \sum_{\ell=1}^N (\exp(-\frac{\lambda t}{N}))^\ell = N/(\lambda t L)$, where ℓ denotes the length of the region occupied by the s permutation.

A simple inspection to Eq. (39) shows that this is a sum of two decaying exponentials in time, with two different rates. For noise rates $\lambda < 1/\tau$, the first term, coinciding with the global fidelity $F = e^{-\lambda t}$, dominates. In this regime therefore, the XEB at large times gives access to the fidelity of the global circuit, whereas for $\lambda > 1/\tau$ the second exponential takes over, giving the noise-independent decay rate $1/\tau$. This is precisely the “transition” already observed in Ref. [3, 30], where it is claimed that the sharp crossover at noise rate $\lambda = \lambda_c$ signals the breakdown of XEB as a proxy for fidelity. This is shown numerically in Fig. 5. We here clarify two points. The first is that the critical value of λ is precisely determined by the scaling of the half-system purity $1/\tau$. The second important point is that *the XEB at late times does provide information about the fidelity F even in the regime $\lambda > 1/\tau$* . It suffices to determine λ by simultaneously fitting λ , τ , and L_0 using the second term of Eq. (39), and then compute the fidelity as usual via $F = e^{-\lambda t}$ (notice that τ may alternatively be extracted from the scaling of the purity, if available).

We use the latter approaches to determine x and λ in order to reconstruct the PoP $P_{x,\lambda t}(w)$ (see Fig. 4). Specifically, we first fit the numerically obtained values of XEB at large times t using Eq. (39), which allows us to extract λ , τ , and L_0 . While one could then directly compute $x(t)$ by assuming the form $x = \frac{N}{L_0} e^{-t/\tau}$, using the fitted values of L_0 and τ , this expression may have extra corrections at early times. In practice, we find improved accuracy by instead adopting the approach used in Section VI: after having found λ , τ , L_0 from the fit, and then invert Eq. (33) to obtain $x = x(t, \text{XEB}, \lambda)$. With both x and λ determined in this way, we reconstruct the analytical distribution $P_{x,\lambda t}(w)$ with moments given by Eq. (32).

VIII. CONCLUSIONS

In this work we have investigated the universal properties of anticoncentration in generic, chaotic quantum many-body systems subject to noise. Whereas the influence of noise on infinite-depth circuits, characterized by the Porter–Thomas distribution of overlaps, has been recently studied, see for example [49], here we have focused on *the interplay between finite circuit depth and noise*, a question of central relevance for near-term quantum devices. We derived a universal form of the distribution of bit-strings probabilities (PoP distribution), as a function of two dimensionless parameters x and η determined by circuit depth, system size, and the global fidelity. As

we have shown, these parameters can be extracted in an experimental setting by evaluating the linear cross entropy XEB across different circuit depths, for any values of noise strength, at least in the regime where the number of error remains subleading $-\log F \ll N$. Given that our interest is in shallow circuits, this regime is achieved even for very strong noise strengths at small depths, and indeed our universal PoP distribution provides an excellent fit of our numerical data for quite shallow circuits and strong noise.

Our analysis is based on an exact mapping to a one-dimensional model of random matrix product operator, that are generated by the action of a generic noisy staircase circuit. Beyond serving as a tractable theoretical toy model, noisy RMPO are themselves experimentally accessible on current quantum platforms [93–97], whereas random MPO can also be used to benchmark of quantum experiments [98]. Thus, our results not only furnish clear predictions for state-of-the-art quantum machines that can be directly used for useful benchmarking, but also clarify the persistence of genuine quantum effects in the presence of realistic noise.

IX. ACKNOWLEDGMENTS

We acknowledge discussions with Xhek Turkeshi and for collaborations on related topics. J.D.N. and G.L. are funded by the ERC Starting Grant 101042293 (HEPIQ) and the ANR-22-CPJ1-0021-01. ADL acknowledges support by the ANR JCJC grant ANR-21-CE47-0003 (TamEnt).

Code and Data Availability. The code and the data for our simulations will be publicly shared at publication.

Appendix A: Derivation of the transfer matrix for single-qudit noise

Here, we provide a full derivation of the replica tensor network for the single-qudit noise RMPO model giving Eq. (17). In Eq. (15), unitaries U_i , of size $d\chi \times d\chi$, act on $r+1$ qudits, with $r = \log_d \chi$. To compute the overlap $w_{\mathbf{x}} = D\langle\langle \mathbf{x}, \mathbf{x} | \rho_N(U) \rangle\rangle$ for a fixed bit-string \mathbf{x} , one must contract the open physical legs in Eq. (15) with the state $\langle\langle \mathbf{x}, \mathbf{x} |$; that is,

$$w_{\mathbf{x}} = D\langle\langle \mathbf{x}, \mathbf{x} | \rho_N(U) \rangle\rangle = D\langle\langle \mathbf{x}, \mathbf{x} | \prod_{i=1}^{N-r} \left(\bigotimes_{j=i}^{i+r} \mathcal{N}_j \right) (U_i \otimes U_i^*) | \mathbf{0}, \mathbf{0} \rangle\rangle, \quad (\text{A1})$$

where $\mathcal{N}_j | \rho \rangle\rangle = |\mathcal{N}_j(\rho) \rangle\rangle = \sum_{\alpha} K_{\alpha} \otimes K_{\alpha}^* | \rho \rangle\rangle$ (we omit dependence on the noise strength γ for readability). To compute the IPR $I_k = D^{-k} \sum_{\mathbf{x}} \mathbb{E}[w_{\mathbf{x}}^k]$, one must replicate the network k times, sum over all \mathbf{x} and perform the average over the U_i . This results in

$$I_k = \mathbb{E}_U \left[\left(\langle\langle \mathbf{x}, \mathbf{x} | \prod_{i=1}^{N-r} \left(\bigotimes_{j=i}^{i+r} \mathcal{N}_j \right) (U_i \otimes U_i^*) | \mathbf{0}, \mathbf{0} \rangle\rangle \right)^{\otimes k} \right]. \quad (\text{A2})$$

Now we employ the Weingarten formula

$$\begin{aligned} \mathbb{E}_{U \sim \text{Haar}(d\chi)} [(U \otimes U^*)^{\otimes k}] &= \\ &= \sum_{\pi, \sigma \in S_k} \text{Wg}_{\pi, \sigma}(d\chi) |\sigma\rangle\rangle_d |\sigma\rangle\rangle_{\chi} \langle\langle \pi |_{\chi} \langle\langle \pi |_d, \end{aligned} \quad (\text{A3})$$

where we explicitly used the factorization $|\sigma\rangle\rangle_{d\chi} = |\sigma\rangle\rangle_d |\sigma\rangle\rangle_{\chi}$. This equation has to be applied for all matrices U_i . At the boundaries, the permutations are either contracted with $|0, 0\rangle$, resulting in an irrelevant factor $\langle\langle \pi | (|0, 0\rangle)^{\otimes k} \rangle\rangle_d^k = 1$, or with the vectors $|x_i, x_i\rangle\rangle$. In this case, the permutations acquire a weight $\langle\langle x_i, x_i |^{\otimes k} \mathcal{N}_{\gamma}^{\otimes k} | \sigma \rangle\rangle_d$. We can incorporate the sum over x_i in this weight and define the $k! \times k!$ matrix $\Lambda_{\sigma' \sigma}(d, \gamma) = \delta_{\sigma' \sigma} \sum_{x_i=0}^{d-1} \langle\langle x_i, x_i |^{\otimes k} \mathcal{N}_{\gamma}^{\otimes k} | \sigma \rangle\rangle_d$, which encodes the weights on the diagonal of the transfer matrix. The last gate of the staircase U_{N-r} has all the $r+1$ output legs contracted with the noise, thus resulting in a weight $R_{\sigma} = (\sum_{x_i=0}^{d-1} \langle\langle x_i, x_i |^{\otimes k} \mathcal{N}_{\gamma}^{\otimes k} | \sigma \rangle\rangle_d)^{r+1}$, which defines the right boundary vector $|R\rangle = \Lambda(d, \gamma)^{r+1} |1 \dots 1\rangle$ of length $k!$. The left boundary vector, instead, is obtained by contracting the permutation obtained from U_1 with the state $|0, 0\rangle$, also incorporating the associated Weingarten coefficients. This results in $|L\rangle = (1 | \text{Wg}(d\chi)$. In the bulk, permutations resulting from consecutive matrices U_i, U_{i+1} are contracted together with r single-qudit noise channels, giving rise to the overlaps matrix $\tilde{G}_{\sigma, \pi}(\chi, \gamma) = \langle\langle \sigma | \mathcal{N}_{\gamma}^{\otimes k} | \pi \rangle\rangle_d^r$. Putting together all these terms one finally obtain Eq. (17), with the transfer matrix defined as in Eq. (18). Notice that in Eq. (17) there are in total $N-r$ Weingarten matrices (one incorporated in $|L\rangle$ and $N-r-1$ in the term T^{N-r-1}), as should be as the staircase circuit Eq. (15) features exactly $N-r$ unitaries.

The derivation of the XEB for this model follows similarly, now involving only $k=2$ replicas: one noisy and one

noiseless. The Weingarten matrix remains unchanged, while the overlap matrix is replaced by

$$[\tilde{G}_{\text{XEB}}]_{\sigma',\sigma}(\chi, \gamma) = \langle\langle \sigma' | \mathcal{N}_\gamma \otimes \mathbb{1} | \sigma \rangle\rangle_d^r, \quad (\text{A4})$$

with $\sigma', \sigma \in S_2$. Calculations analogous to those in Section IV then yield

$$\tilde{G}_{\text{XEB}}(\chi, \gamma) = \chi^2 \begin{pmatrix} 1 & 1/\chi \\ 1/\chi & 1 - \eta/N \end{pmatrix}, \quad (\text{A5})$$

where we used Eq. (29). This equation is the analogous of Eq. (28). As for I_2 , we can write the replica contraction $\text{XEB} = D(L|T_{\text{XEB}}^{N-r-1}|R) - 1$ with $T_{\text{XEB}} = \Lambda_{\text{XEB}}(d, \gamma)\tilde{G}_{\text{XEB}}(\chi, \gamma)\text{Wg}(d\chi)$. Once again, the matrix $[\Lambda_{\text{XEB}}]_{\sigma'\sigma}(d, \gamma) = \delta_{\sigma'\sigma} \sum_{x_i=0}^{d-1} \langle\langle x_i, x_i | \otimes^2 \mathcal{N}_\gamma \otimes \mathbb{1} | \sigma \rangle\rangle_d = d\delta_{\sigma'\sigma}(1 + O(\gamma))$ in the scaling limit becomes effectively proportional to the identity matrix, giving only a trivial contribution. In this limit, the boundary vectors (L) and (R) are also the same as for I_2 . Hence, we get

$$T_{\text{XEB}} = d^{-1} \left(\mathbb{1} + \frac{x}{N} A - \frac{\eta}{2N} Q + O(N^{-2}) \right), \quad (\text{A6})$$

which, in the scaling limit and after exponentiation, leads to Eq. (33).

The calculation of the average state fidelity $F = \mathbb{E}_U[\text{Tr}(\rho_N(U)\rho(U))]$ is very similar to the one of XEB. The trace in the fidelity expression can be evaluated using the ‘swap trick’ by rewriting $\text{Tr}(\rho_N\rho) = \text{Tr}((\rho_N \otimes \rho)s) = \langle\langle \rho_N \otimes \rho | s \rangle\rangle$, where s denotes here the swap operator (or equivalently the transposition permutation). This modifies the matrix previously called Λ_{XEB} into $[\Lambda_F]_{\sigma'\sigma}(d, \gamma) = \delta_{\sigma'\sigma} \langle\langle s | \mathcal{N}_\gamma \otimes \mathbb{1} | \sigma \rangle\rangle_d$, so that the replica contraction now reads $F = (L|T_F^{N-r-1}|R)$ with $T_F = \Lambda_F(d, \gamma)\tilde{G}_{\text{XEB}}(\chi, \gamma)\text{Wg}(d\chi)$. As before, the noise inside Λ_F does not play any role in the scaling limit, therefore $[\Lambda_F]_{\sigma'\sigma}(d, \gamma) \stackrel{\text{s.l.}}{=} \delta_{\sigma'\sigma} \langle\langle s | \sigma \rangle\rangle_d$ and $\Lambda_F(d, \gamma) \stackrel{\text{s.l.}}{=} \text{diag}(d, d^2)$. Finally, we get

$$T_F \stackrel{\text{s.l.}}{=} \begin{pmatrix} 1/d & x/(dN) \\ x/N & 1 - \eta/N \end{pmatrix}, \quad (\text{A7})$$

which in the scaling limit yields $F \stackrel{\text{s.l.}}{=} e^{-\eta}$.

Appendix B: RMPO with multi-qudit noise

Here, we consider an alternative model of noisy RMPO, in which the noise acts collectively on all $r+1$ qudits within each layer of the staircase circuit ($r = \log_d \chi$),

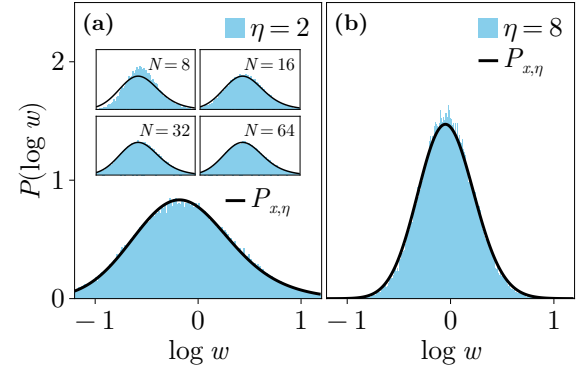
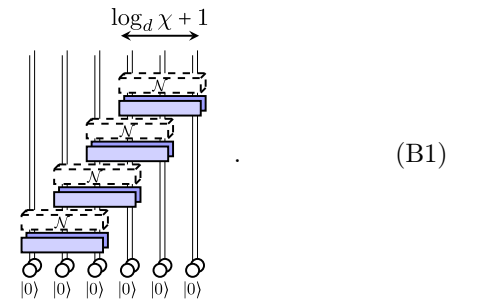


Figure 6. PoP of RMPO for construction of Eq. (B1) for $N = 128$, $\chi = 128$ ($x = 0.5$), and $2 \leq \eta \leq 8$. The distribution of $\log w$ can be approximated as a Gram-Charlier A series (black line) where only the first two terms of the expansion have been considered and the cumulants of the distribution have been fitted from I_k computed from Eq. (32) for $k \in \{1, \dots, 6\}$. Inset of panel (a) shows the approach to the universal prediction by increasing N .

as illustrated here



We show that, in the weak-noise regime, this model is also described by the same transfer matrix. In the vectorized formalism, the combined action of the unitary gates followed by the noise is $\mathcal{N}_\gamma((U \otimes U^*)|\rho\rangle\rangle)$, where ρ is a certain trial density matrix. For simplicity, we assume here a specific form of noise, namely the depolarizing channel $\mathcal{N}_\gamma^{\text{dep.}}(\rho) = (1 - \gamma)\rho + \gamma \frac{1}{q}$, where q is the Hilbert space dimension on which $\mathcal{N}_\gamma^{\text{dep.}}$ acts on. In our case, $q = d\chi = d^{r+1}$ and

$$\mathcal{N}_\gamma^{\text{dep.}}((U \otimes U^*)|\rho\rangle\rangle) = (1 - \gamma)(U \otimes U^*)|\rho\rangle\rangle + \frac{\gamma}{q}|e\rangle\rangle\langle\langle e|\rho\rangle\rangle, \quad (\text{B2})$$

where e is the identity permutation (which contracted with ρ gives $\langle\langle e|\rho\rangle\rangle = \text{Tr}[\rho]$). Since we want to perform replica calculations, i.e. averaging k -replicas of Eq. (B1), the crucial quantity of interest is for us

$$\begin{aligned} \mathbb{E}_U[(\mathcal{N}_\gamma^{\text{dep.}}((U \otimes U^*)|\rho\rangle\rangle))^{\otimes k}] &= \\ &= \mathbb{E}_U[((1 - \gamma)U \otimes U^* + \frac{\gamma}{q}|e\rangle\rangle\langle\langle e|)^{\otimes k}]|\rho\rangle\rangle^{\otimes k}, \end{aligned} \quad (\text{B3})$$

where, by linearity, the trial density matrix is taken outside the average. We now assume the following form

$$\begin{aligned} \mathbb{E}_U & \left[\left((1-\gamma) U \otimes U^* + \frac{\gamma}{q} |e\rangle\langle e| \right)^{\otimes k} \right] = \\ & = \sum_{\pi, \sigma \in S_k} \tilde{W}g_{\pi, \sigma}(q, \gamma) |\sigma\rangle\langle\pi|, \end{aligned} \quad (\text{B4})$$

which is justified in analogy with Eq. (6), and where $\tilde{W}g_{\pi, \sigma}(q, \gamma)$ denotes *noisy Weingarten coefficients* that remain to be determined.

To find these coefficients, we fix σ and π , and observe that each common fixed point of the two permutations can be obtained in the expansion of the left-hand side of Eq. (B4) from a term $|e\rangle\langle e|$ appearing in a specific position, while the remaining part of the two permutations should be obtained from the average of $U \otimes U^*$. Taking these observations into account, we arrive at

$$\tilde{W}g_{\pi, \sigma}(q, \gamma) = \sum_{i=0}^{n_F(\pi, \sigma)} \binom{n_F(\pi, \sigma)}{i} \frac{\gamma^i}{q^i} (1-\gamma)^{k-i} Wg_{\tilde{\pi}(i), \tilde{\sigma}(i)}^{(k-i)}(q), \quad (\text{B5})$$

where $n_F(\pi, \sigma)$ denotes the number of common fixed points between π and σ , and $\tilde{\pi}(i)$, $\tilde{\sigma}(i)$ denote the permutations obtained from π , σ , respectively, by removing i of these common fixed points (which ones is unimportant, because Wg depends only the cycle structure).

We can now compute the IPR I_k and expressing it, in analogy with Eq. (17), as

$$I_k = D(L|T^{N-r-1}|R) \quad (\text{B6})$$

where now the transfer matrix is $T = G(\chi) \tilde{W}g(d\chi, \gamma)$, $(L| = (1|\tilde{W}g(d\chi, \gamma)$ and $|R) = |1)$. As in the main text, we focus on the scaling limit $N, \chi \rightarrow \infty$, $\gamma \rightarrow 0$ with $x \propto N/\chi$ and $\eta \propto \gamma N$ fixed. In this regime, it is sufficient to expand the transfer matrix to first order in $1/\chi$ and γ , which is equivalent to retaining only the leading-order terms in $1/N$. Noting that, in Eq. (B5), only the terms with $i = 0, 1$ contribute at this order, we obtain

$$\tilde{W}g(d\chi, \gamma) = (d\chi)^{-k} \left(1 - \frac{1}{d-1} \frac{x}{N} A - \frac{\eta}{N} Q + O(N^{-2}) \right), \quad (\text{B7})$$

which is analogous to Eq. (28) in the main text and where we set

$$\gamma = \frac{\eta}{N}. \quad (\text{B8})$$

Hence, the transfer matrix in Eq. (17) can be written as

$$T = d^{-k} \left(1 + \frac{1}{N} (xA - \eta Q) + O(N^{-2}) \right), \quad (\text{B9})$$

which allows to recover Eq. (32) in the scaling limit.

In Fig. 6, we present the PoP distribution of noisy

RMPO constructed as in Eq. (B1) for a specific value of x and various values of η . There is a strong agreement between the experimental distribution and the Gram-Charlier A series. Furthermore, in Fig. 6(a), we illustrate how the data approach the Gram-Charlier expansion as the system size N increases.

In this framework, as in Appendix A, we can also compute the average state fidelity $F = \mathbb{E}[\text{Tr}(\rho_N \rho)] = \langle \rho_N \otimes \rho | s \rangle$ for the circuit shown in Eq. (B1), where the average is over all random unitary gates. For this quantity, we need to average two replicas of the circuit, one noiseless and the other noisy. Therefore, we can formally define new Weingarten coefficients $[\tilde{W}g_F]_{\pi, \sigma}(q, \gamma)$ through the equality

$$\begin{aligned} \mathbb{E}_U & \left[\left((1-\gamma) U \otimes U^* + \frac{\gamma}{q} |e\rangle\langle e| \right) \otimes (U \otimes U^*) \right] = \\ & = \sum_{\pi, \sigma \in S_k} [\tilde{W}g_F]_{\pi, \sigma}(q, \gamma) |\sigma\rangle\langle\pi|. \end{aligned} \quad (\text{B10})$$

The modified Weingarten matrix $\tilde{W}g_F$ can be computed in a similar way as above, with the notable simplification that only two replicas are involved in this case. In the identity-swap $\{e, s\}$ basis this matrix reads

$$\tilde{W}g_F(q, \gamma) = \begin{pmatrix} \frac{1-\gamma}{q^2-1} + \frac{\gamma}{q^2} & -\frac{1-\gamma}{q(q^2-1)} \\ -\frac{1-\gamma}{q(q^2-1)} & \frac{1-\gamma}{q^2-1} \end{pmatrix}. \quad (\text{B11})$$

The contraction with the swap operator s brings a weight to each permutation given by the diagonal matrix $[\Lambda_F]_{\sigma' \sigma}(d) = \delta_{\sigma' \sigma} \langle s | \sigma \rangle_d$. As for the IPRs, we can then write the fidelity F as a matrix contraction in the space of permutations, namely $F = (L_F | T_F^{N-r-1} | R_F)$ with the transfer matrix defined as $T_F = \Lambda_F(d) G(\chi) \tilde{W}g_F(d\chi, \gamma)$, and boundary vectors $(L_F| = (1| \tilde{W}g_F(d\chi, \gamma)$ and $|R_F) = |1)$. By keeping $x = \frac{d-1}{d} \frac{N}{\chi}$ and $\eta = \gamma N$ fixed and taking the large N limit, we see that to first order in $1/N$, we can write

$$T_F = \begin{pmatrix} \frac{1}{d} & \frac{x}{dN} \\ \frac{x}{N} & 1 - \frac{\eta}{N} \end{pmatrix} + O(1/N^2). \quad (\text{B12})$$

Finally, we get $F \stackrel{\text{s.l.}}{\equiv} \lim_{N \rightarrow \infty} (1 - \frac{\eta}{N})^N = e^{-\eta}$. Moreover, the calculation of the XEB is similar to the one of I_2 , except the Weingarten matrix is now given by Eq. (B11). This gives the universal Eq. (33).

Appendix C: Random phase model

To begin, let us briefly revisit the standard definition of the Random Phase Model (RPM) [44, 67]. This model consists of a random circuit acting on N qudits and defined the subsequent action of two different layers at time step t : first, on each site i , one acts with single-site Haar-random unitary, $U_i^{(1)}(t)$; then, on each bond between neighboring sites $(j, j+1)$, one acts

with a diagonal two-site gate whose entries are phases $[U_{j,j+1}^{(2)}(t')]_{x_j x_{j+1}, x_j x_{j+1}} = \exp[i\varphi_{x_j, x_{j+1}}^{(j)}(t')]$ ($x_j, x_{j+1} \in \{0, 1, \dots, d-1\}$). Each phase $\varphi_{x_j, x_{j+1}}^{(j)}(t')$ is an independent Gaussian random real variable with mean zero and variance ϵ , which controls the coupling strength between neighboring spins. A given realization of the circuit is obtained by drawing independently for each j and t' the single-site unitaries and the phases $\varphi_{x_j, x_{j+1}}^{(j)}(t')$. Consider the k -th moment of the output distribution $w^k = D\langle \mathbf{x} | W_{\text{RPM}}(t) | \mathbf{x} \rangle$, where $W_{\text{RPM}}(t)$ denotes the global RPM circuit with t repeated action of single-site and two-site layers. As explained in [44], the circuit average $\mathbb{E}[w^k]$ in the absence of noise can be computed at large d in two steps: one first averages over the single-site unitaries using once again the Weingarten formula

$$\begin{aligned} \mathbb{E}_{\text{RPM}}[(U_i^{(1)}(t') \otimes U_i^{(1)}(t')^*)^{\otimes k}] &= \\ &= \sum_{\pi, \sigma \in S_k} \text{Wg}_{\pi, \sigma}(d) |\sigma\rangle_d \langle \pi|_d = d^{-k} \sum_{\sigma \in S_k} |\sigma\rangle_d \langle \sigma|_d \end{aligned} \quad (\text{C1})$$

Note that this equation is formally analogous to (6), but it is restricted to the action on the d -dimensional local physical Hilbert space. Beyond allowing the expansion of Weingarten functions, the large d limit also implies that the same permutation $\sigma_i \in S_k$ at a given site i propagates at all times, as the overlaps $G_{\sigma', \sigma}(d) = \langle \sigma' | \sigma \rangle_d \sim d^k \delta_{\sigma', \sigma}$. Thus, the effect of the 2-site gates can be accounted for computing

$$\langle\langle \sigma_j, \sigma_{j+1} | U_{j,j+1}^{(2)}(t') | \sigma_j \sigma_{j+1} \rangle\rangle = d^{2k} e^{-\epsilon(k - n_F(\sigma_j, \sigma_{j+1}))}, \quad (\text{C2})$$

where $n_F(\sigma_j, \sigma_{j+1})$ denotes the number of common fixed points between σ_j and σ_{j+1} . Collecting the contribution from the t layers of phases, we have that

$$\mathbb{E}[w^k] = \sum_{\sigma, \sigma'} [T_{\text{RPM}}^N]_{\sigma, \sigma'}, \quad [T_{\text{RPM}}]_{\sigma', \sigma} = e^{-\epsilon t(k - n_F(\sigma, \sigma'))} \quad (\text{C3})$$

In order to include the effect of noise, we assume for simplicity that it affects each single-site Haar unitary, with the presence of a depolarizing channel $\mathcal{N}_\gamma^{\text{dep}}$. Consequently, as in Eq. (B4), we replace $\text{Wg}(d)$ with $\tilde{\text{Wg}}(d, \gamma)$ in (C1). For large d , Eq. (B7) yields

$$\tilde{\text{Wg}}(d, \gamma) = d^{-k} (1 - \gamma Q + O(\gamma^2) + O(d^{-1})). \quad (\text{C4})$$

We thus arrive at

$$\mathbb{E}[w^k] = \sum_{\sigma, \sigma'} [\tilde{T}_{\text{RPM}}^N]_{\sigma, \sigma'}, \quad \tilde{T}_{\text{RPM}} = T_{\text{RPM}} e^{-Q\gamma t + O(\gamma^2)} \quad (\text{C5})$$

Now, we recall that for the RPM, the Thouless length can be identified with $L(t) = e^{2\epsilon t}$ and at large time, one can rewrite

$$T_{\text{RPM}} = 1 + \frac{A}{L(t)} + O(L(t)^{-2}) \sim e^{A/L(t)}. \quad (\text{C6})$$

Finally, in the scaling limit (1) and $\gamma = \eta/(Nt)$, we can combine the two factors in $\tilde{T}_{\text{RPM}}^N \sim [e^{Ax/N} e^{-Q\eta/N}]^N \rightarrow e^{Ax - Q\eta}$, in agreement with (32) in the main text.

Appendix D: Additional numerical data

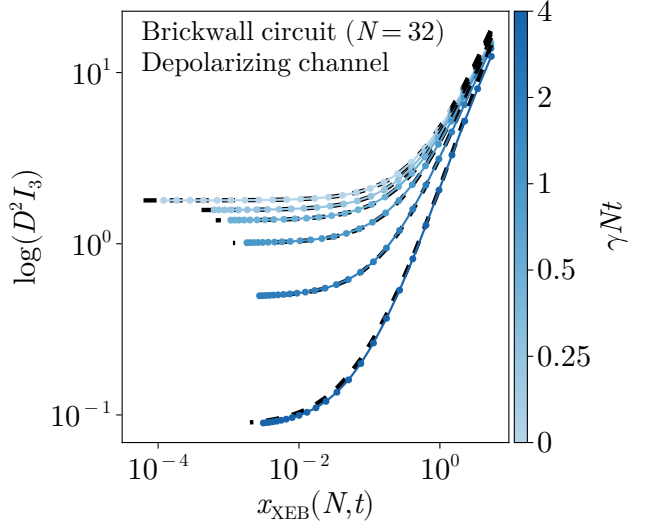


Figure 7. Plot of I_3 for the brickwall circuit with two-qubits depolarizing channel with noise strength $\gamma \propto 1/(Nt)$, with $N = 32$. We show it as a function of $x_{\text{XEB}}(N, t)$ which is obtained by computing first the XEB at large time to estimate η and then by computing the XEB at time t , and inverting Eq. (33) to obtain x . We show also the analytical prediction Eq. (32) (black dashed line).

In Fig. 7, we show I_3 for the brickwall circuit. The plot is analogous to the plot of XEB in Fig. 2. We show that the x extracted from the XEB, with the procedure detailed in the main text, gives good predictions beyond 2-replicas observables through Eq. (32). This provides an additional check that all the moments of the anticoncentration, namely the whole PoP distribution, depend only on the two fitting parameters η and x .

In Fig. 8, we show that the average half-chain purity

$$P_{N/2} = \mathbb{E}[\text{Tr}(\rho_{N/2}^2)], \quad (\text{D1})$$

with $\rho_{N/2} = \text{Tr}_{1, \dots, N/2}(\rho_N(U))$, scales as $e^{-t(\lambda+1/\tau)}$. This observation comes from the fact that we can write $P_{N/2} = \text{Tr}(\rho^{\otimes 2}(s^{\otimes N/2} \otimes 1^{\otimes N/2}))$, where s is the swap operator. This forces a unique domain configuration

$$\overbrace{\quad \quad \quad}^s \overbrace{\quad \quad \quad}^e. \quad (\text{D2})$$

The contribution of the identity e is 1 while the contribution of the swap s is $\lim_{N \rightarrow \infty} (1 - \frac{\eta t}{N} Q_{ss})^{N/2} = e^{-\eta t}$. The unique domain wall gives $L^{-1} = L_0^{-1} e^{-t/\tau}$. Collecting all these contributions gives the correct scaling.

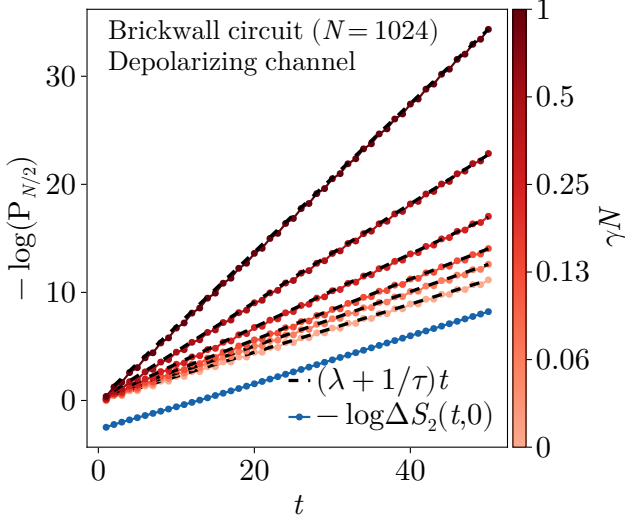


Figure 8. Scaling of the half-chain purity for the brickwall circuit with two-qubits depolarizing channel and noise strength $\gamma \propto 1/N$. The system size is $N = 1024$. We show that this scaling is $\exp(-t \cdot (\lambda + 1/\tau))$, where the parameter λ is obtained through a fit from the XEB at large times. τ , given by Eq. (35), is the scaling of the purity in the noiseless case $\lambda = 0$. It also corresponds to the scaling of $\Delta S_2(t,0) = S_2(\infty,0) - S_2(t,0)$ (see blue line), where $S_2(t, \lambda) = -\log I_2(t, \lambda)$ is the participation entropy and $S_2(\infty, 0) = -\log I_2^{\text{PT}}$. (For visualization purposes, the blue line is shifted by a constant of 3).

[1] F. Arute, K. Arya, R. Babbush, D. Bacon, J. C. Bardin, R. Barends, R. Biswas, S. Boixo, F. G. Brandao, D. A. Buell, *et al.*, [Nature 574, 505–510 \(2019\)](#).

[2] S. Boixo, S. V. Isakov, V. N. Smelyanskiy, R. Babbush, N. Ding, Z. Jiang, M. J. Bremner, J. M. Martinis, and H. Neven, [Nature Phys. 14, 595–600 \(2018\)](#).

[3] A. Morvan, B. Villalonga, and X. e. a. Mi, [Nature 634, 328–333 \(2024\)](#).

[4] L. Daguerre, R. Blume-Kohout, N. C. Brown, D. Hayes, and I. H. Kim, Experimental demonstration of high-fidelity logical magic states from code switching (2025), [arXiv:2506.14169](#).

[5] M. Liu, R. Shaydulin, P. Niroula, M. DeCross, S.-H. Hung, W. Y. Kon, E. Cervero-Martín, K. Chakraborty, O. Amer, S. Aaronson, A. Acharya, Y. Alexeev, K. J. Berg, S. Chakrabarti, F. J. Curchod, J. M. Dreiling, N. Erickson, C. Foltz, M. Foss-Feig, D. Hayes, T. S. Humble, N. Kumar, J. Larson, D. Lykov, M. Mills, S. A. Moses, B. Neyenhuis, S. Eloul, P. Siegfried, J. Walker, C. Lim, and M. Pistoia, [Nature 640, 343–348 \(2025\)](#).

[6] Z. Yin, I. Agresti, G. de Felice, D. Brown, A. Toumi, C. Pentangelo, S. Piacentini, A. Crespi, F. Ceccarelli, R. Osellame, B. Coecke, and P. Walther, [Nature Photonics 10.1038/s41566-025-01682-5 \(2025\)](#).

[7] R. Haghshenas, E. Chertkov, M. Mills, W. Kadow, S.-H. Lin, Y.-H. Chen, C. Cade, I. Niesen, T. Begušić, M. S. Rudolph, C. Cirstoiu, K. Hemery, C. M. Keever, M. Lubasch, E. Granet, C. H. Baldwin, J. P. Bartolotta, M. Bohn, J. Cline, M. DeCross, J. M. Dreiling, *et al.*, Digital quantum magnetism at the frontier of classical simulations (2025), [arXiv:2503.20870](#).

[8] L. Shirizly, G. Misguich, and H. Landa, [Phys. Rev. Lett. 132, 010601 \(2024\)](#).

[9] M. C. Smith, A. D. Leu, K. Miyanishi, M. F. Gely, and D. M. Lucas, [Phys. Rev. Lett. 134, 230601 \(2025\)](#).

[10] B. Rost, L. Del Re, N. Earnest, A. F. Kemper, B. Jones, and J. K. Freericks, [npj Quantum Information 11, 10.1038/s41534-025-00964-8 \(2025\)](#).

[11] M. Ringbauer, M. Hinsche, T. Feldker, P. K. Faehrmann, J. Bermejo-Vega, C. L. Edmunds, L. Postler, R. Stricker, C. D. Marciak, M. Meth, I. Pogorelov, R. Blatt, P. Schindler, J. Eisert, T. Monz, and D. Hangleiter, [Nature Communications 16, 10.1038/s41467-024-55342-3 \(2025\)](#).

[12] C. Cafaro and S. Mancini, [Phys. Rev. A 82, 012306 \(2010\)](#).

[13] J. Preskill, [Quantum 2, 79 \(2018\)](#).

[14] B. M. Terhal, [Rev. Mod. Phys. 87, 307 \(2015\)](#).

[15] D. Aasen, M. Aghaee, Z. Alam, M. Andrzejczuk, A. Antipov, M. Astafev, L. Avilovas, A. Barzegar, B. Bauer, J. Becker, J. M. Bello-Rivas, U. Bhaskar, A. Bocharov, S. Boddapati, D. Bohn, *et al.*, [Roadmap to fault toler-](#)

ant quantum computation using topological qubit arrays (2025), arXiv:2502.12252 [quant-ph].

[16] T. Peham, L. Schmid, L. Berent, M. Müller, and R. Wille, *PRX Quantum* **6**, 020330 (2025).

[17] J. C. Napp, R. L. La Placa, A. M. Dalzell, F. G. S. L. Brandão, and A. W. Harrow, *Phys. Rev. X* **12**, 021021 (2022).

[18] J. Chen, F. Zhang, C. Huang, M. Newman, and Y. Shi, arXiv preprint arXiv:1805.01450 (2018).

[19] I. L. Markov, A. Fatima, S. V. Isakov, and S. Boixo, arXiv preprint arXiv:1807.10749 (2018).

[20] C. Huang, F. Zhang, M. Newman, J. Cai, X. Gao, Z. Tian, J. Wu, H. Xu, H. Yu, B. Yuan, M. Szegedy, Y. Shi, and J. Chen, *Classical simulation of quantum supremacy circuits* (2020), arXiv:2005.06787 [quant-ph].

[21] S. Aaronson and L. Chen, Complexity-theoretic foundations of quantum supremacy experiments (2016), arXiv:1612.05903 [quant-ph].

[22] V. Pednault, J. A. Gunnels, G. Nannicini, L. Horesh, and R. Wisnieff, Leveraging secondary storage to simulate deep 54-qubit sycamore circuits (2019).

[23] J. Gray and S. Kourtis, *Quantum* **5**, 410 (2021).

[24] S. Bravyi, D. E. Browne, P. Calpin, E. Campbell, D. Gosset, and M. Howard, arXiv preprint arXiv:1808.00128 (2018).

[25] T. Vincent, L. J. O’Riordan, M. Andrenkov, J. Brown, N. Killoran, H. Qi, and I. Dhand, arXiv preprint arXiv:2107.09793 (2021).

[26] R. Harper, S. T. Flammia, and J. J. Wallman, *Nature Physics* **16**, 1184–1188 (2020).

[27] S. Hohloch and J. Palmer, Extending compact hamiltonian \mathbb{S}^1 -spaces to integrable systems with mild degeneracies in dimension four (2021), arXiv:2105.00523.

[28] J. Choi, A. L. Shaw, I. S. Madjarov, X. Xie, R. Finkelstein, J. P. Covey, J. S. Cotler, D. K. Mark, H.-Y. Huang, A. Kale, H. Pichler, F. G. S. L. Brandão, S. Choi, and M. Endres, *Nature* **613**, 468–473 (2023).

[29] X. Gao, M. Kalinowski, C.-N. Chou, M. D. Lukin, B. Barak, and S. Choi, *PRX Quantum* **5**, 10.1103/prxquantum.5.010334 (2024).

[30] B. Ware, A. Deshpande, D. Hangleiter, P. Niroula, B. Feferman, A. V. Gorshkov, and M. J. Gullans, *A sharp phase transition in linear cross-entropy benchmarking* (2023), arXiv:2305.04954 [quant-ph].

[31] S. Liu, M.-R. Li, S.-X. Zhang, S.-K. Jian, and H. Yao, *Physical Review B* **110**, 10.1103/physrevb.110.064323 (2024).

[32] D. K. Mark, J. Choi, A. L. Shaw, M. Endres, and S. Choi, *Phys. Rev. Lett.* **131**, 110601 (2023).

[33] M. P. Fisher, V. Khemani, A. Nahum, and S. Vijay, *Annual Review of Condensed Matter Physics* **14**, 335–379 (2023).

[34] A. W. Harrow and R. A. Low, *Communications in Mathematical Physics* **291**, 257 (2009).

[35] F. G. S. L. Brandão, A. W. Harrow, and M. Horodecki, *Communications in Mathematical Physics* **346**, 397 (2016).

[36] D. Hangleiter, J. Bermejo-Vega, M. Schwarz, and J. Eisert, *Quantum* **2**, 65 (2018).

[37] A. M. Dalzell, N. Hunter-Jones, and F. G. S. L. Brandão, *PRX Quantum* **3**, 010333 (2022).

[38] D. J. Luitz, N. Laflorencie, and F. Alet, *J. Stat. Mech.: Theor. Exp.* **2014**, P08007 (2014).

[39] D. J. Luitz, F. Alet, and N. Laflorencie, *Phys. Rev. Lett.* **112**, 057203 (2014).

[40] E. Tirrito, X. Turkeshi, and P. Sierant, *Anticoncentration and magic spreading under ergodic quantum dynamics* (2024), arXiv:2412.10229 [quant-ph].

[41] N. Macé, F. Alet, and N. Laflorencie, *Phys. Rev. Lett.* **123**, 180601 (2019).

[42] A. Sauliere, B. Magni, G. Lami, X. Turkeshi, and J. De Nardis, *Universality in the anticoncentration of chaotic quantum circuits* (2025), arXiv:2503.00119 [quant-ph].

[43] G. Lami, J. De Nardis, and X. Turkeshi, *Physical Review Letters* **134**, 10.1103/physrevlett.134.010401 (2025).

[44] A. Christopoulos, A. Chan, and A. De Luca, *Universal distributions of overlaps from generic dynamics in quantum many-body systems* (2025), arXiv:2404.10057 [cond-mat.stat-mech].

[45] B. Magni, A. Christopoulos, A. De Luca, and X. Turkeshi, *Anticoncentration in clifford circuits and beyond: From random tensor networks to pseudo-magic states* (2025), arXiv:2502.20455.

[46] P. W. Claeys and G. De Tomasi, *Phys. Rev. Lett.* **134**, 050405 (2025).

[47] D. K. Mark, F. Surace, A. Elben, A. L. Shaw, J. Choi, G. Refael, M. Endres, and S. Choi, *Phys. Rev. X* **14**, 041051 (2024).

[48] A. Kaufman, J. Corona, Z. Ozzello, B. Senseman, M. Asaduzzaman, and Y. Meurice, *Improved entanglement entropy estimates from filtered bitstring probabilities* (2024), arXiv:2411.07092.

[49] A. L. Shaw, D. K. Mark, J. Choi, R. Finkelstein, P. Scholl, S. Choi, and M. Endres, *Universal fluctuations and noise learning from hilbert-space ergodicity* (2024), arXiv:2403.11971 [quant-ph].

[50] A. De Luca and A. Scardicchio, *Europhysics Letters* **101**, 37003 (2013).

[51] N. Macé, F. Alet, and N. Laflorencie, *Phys. Rev. Lett.* **123**, 180601 (2019).

[52] C. E. Porter and R. G. Thomas, *Phys. Rev.* **104**, 483 (1956).

[53] A. M. Dalzell, N. Hunter-Jones, and F. G. S. L. Brandão, *Communications in Mathematical Physics* **405**, 10.1007/s00220-024-04958-z (2024).

[54] A. Chan, A. De Luca, and J. T. Chalker, *Phys. Rev. Lett.* **121**, 060601 (2018).

[55] S. Shivam, A. De Luca, D. A. Huse, and A. Chan, *Physical Review Letters* **130**, 10.1103/physrevlett.130.140403 (2023).

[56] A. Chan, S. Shivam, D. A. Huse, and A. De Luca, *Nature Communications* **13**, 10.1038/s41467-022-34318-1 (2022).

[57] X. Turkeshi and P. Sierant, *Entropy* **26**, 471 (2024).

[58] S. Garnerone, T. R. de Oliveira, and P. Zanardi, *Phys. Rev. A* **81**, 032336 (2010).

[59] S. Garnerone, T. R. de Oliveira, S. Haas, and P. Zanardi, *Phys. Rev. A* **82**, 052312 (2010).

[60] D. Haag, F. Baccari, and G. Styliaris, *PRX Quantum* **4**, 030330 (2023).

[61] C. Lancien and D. Pérez-García, *Annales Henri Poincaré* **23**, 141–222 (2021).

[62] G. Lami, T. Haug, and J. De Nardis, *PRX Quantum* **6**, 010345 (2025).

[63] Z. Cheng, X. Feng, and M. Ippoliti, *Phys. Rev. Lett.* **135**, 020403 (2025).

[64] A. Nahum, S. Vijay, and J. Haah, *Physical Review X* **8**, 021014 (2018).

[65] L. Logarić, S. Dooley, S. Pappalardi, and J. Goold, [Phys. Rev. Lett. **132**, 010401 \(2024\)](#).

[66] A. Chan, A. De Luca, and J. Chalker, [Physical Review X **8**, 041019 \(2018\)](#).

[67] A. Chan, A. De Luca, and J. Chalker, [Physical Review Letters **121**, 060601 \(2018\)](#).

[68] A. Chan, A. De Luca, and J. Chalker, [Physical Review Letters **122**, 220601 \(2019\)](#).

[69] B. Bertini, P. Kos, and T. Prosen, [Physical Review Letters **123**, 210601 \(2019\)](#).

[70] L. Piroli, B. Bertini, J. Cirac, and T. Prosen, [Physical Review B **101**, 094304 \(2020\)](#).

[71] D. E. Parker, H. Cao, B. Swingle, and X.-L. Qi, [Physical Review X **9**, 041017 \(2019\)](#).

[72] J. S. Cotler, N. Hunter-Jones, J. Liu, B. Yoshida, and X.-L. Qi, [Journal of High Energy Physics **2017**, 48 \(2017\)](#).

[73] K. Khanna, A. Kumar, R. Vasseur, and A. W. W. Ludwig, [Random quantum circuits with time-reversal symmetry \(2025\)](#), [arXiv:2501.13161](#).

[74] F. Barratt, U. Agrawal, S. Gopalakrishnan, D. A. Huse, R. Vasseur, and A. C. Potter, [Phys. Rev. Lett. **129**, 120604 \(2022\)](#).

[75] N. Hunter-Jones, J. Cotler, J. Liu, B. Yoshida, and X.-L. Qi, [Journal of High Energy Physics **2018**, 121 \(2018\)](#).

[76] A. M. Dalzell, N. Hunter-Jones, and F. G. S. L. Brandão, [Random quantum circuits transform local noise into global white noise \(2021\)](#), [arXiv:2111.14907 \[quant-ph\]](#).

[77] G. Köstenberger, [Weingarten Calculus \(2021\)](#), [arXiv:2101.00921 \[math.PR\]](#).

[78] B. Collins, S. Matsumoto, and J. Novak, [Notices of the American Mathematical Society **69**, 1 \(2022\)](#).

[79] R. Brualdi, [Introductory Combinatorics](#), Pearson Education (Pearson Prentice Hall, 2012).

[80] T. Zhou and A. Nahum, [Phys. Rev. B **99**, 174205 \(2019\)](#).

[81] T. Zhou and A. Nahum, [Phys. Rev. X **10**, 031066 \(2020\)](#).

[82] A. De Luca, C. Liu, A. Nahum, and T. Zhou, [Universality classes for purification in nonunitary quantum processes \(2023\)](#), [arXiv:2312.17744 \[cond-mat.stat-mech\]](#).

[83] C. Schon, K. Hammerer, M. M. Wolf, J. I. Cirac, and E. Solano, [Phys. Rev. A **75**, 032311 \(2007\)](#).

[84] H.-P. Breuer and F. Petruccione, [The theory of open quantum systems](#) (OUP Oxford, 2002).

[85] More precisely, the number of noise channels is $(N-r)(r+1)$.

[86] A. Nahum, J. Ruhman, S. Vijay, and J. Haah, [Phys. Rev. X **7**, 031016 \(2017\)](#).

[87] G. Vidal, [Physical Review Letters **93**, 040502 \(2004\)](#).

[88] M. Zwolak and G. Vidal, [Physical Review Letters **93**, 207205 \(2004\)](#).

[89] F. Verstraete, J. J. García-Ripoll, and I. Cirac, [Physical Review Letters **93**, 207204 \(2004\)](#).

[90] M. Fishman, S. R. White, and E. M. Stoudenmire, [SciPost Phys. Codebases , 4 \(2022\)](#).

[91] J. P. Gram, [Matematisk-fysiske Meddelelser fra Det Kongelige Danske Videnskabernes Selskab **6**, 1 \(1883\)](#).

[92] C. V. L. Charlier, [Acta Mathematica **29**, 309 \(1905\)](#).

[93] L. Piroli, G. Styliaris, and J. I. Cirac, [Phys. Rev. Lett. **127**, 220503 \(2021\)](#).

[94] D. Malz, G. Styliaris, Z.-Y. Wei, and J. I. Cirac, [Phys. Rev. Lett. **132**, 040404 \(2024\)](#).

[95] K. C. Smith, A. Khan, B. K. Clark, S. M. Girvin, and T.-C. Wei, [arXiv:2404.16083](#).

[96] D. T. Stephen and O. Hart, [arXiv:2404.16360](#).

[97] Y. Zhang, S. Gopalakrishnan, and G. Styliaris, [arXiv:2405.09615](#).

[98] M. Votto, M. Ljubotina, C. Lancien, J. I. Cirac, P. Zoller, M. Serbyn, L. Piroli, and B. Vermersch, [Learning mixed quantum states in large-scale experiments \(2025\)](#), [arXiv:2507.12550](#).